International Journal of Pressure Vessels and Piping 156 (2017) 23–39

Contents lists available at ScienceDirect

International Journal of Pressure Vessels and Piping

journal homepage: www.elsevier.com/locate/ijpvp

Low constraint fracture toughness testing using SE(T) and SE(B) specimens

Claudio Ruggieri

Department of Naval Architecture and Ocean Engineering, University of São Paulo, São Paulo, Brazil

ARTICLE INFO

Article history:
Received 24 March 2017
Received in revised form
13 July 2017
Accepted 13 July 2017
Available online 19 July 2017

Keywords:
J-resistance curves
Constraint effects
SE(T) specimen
SE(B) specimen
Pipeline girth weld

ABSTRACT

This work presents a brief review of current progress in fracture resistance test procedures to measure crack growth properties of pipeline steels using clamped SE(T) and shallow-crack SE(B) specimens. A central objective is to assess recently developed practices for *J* and CTOD resistance curve test methods with particular emphasis on the estimation procedures for *J* and CTOD as well as the experimental evaluation of stable crack growth. An overview of the fracture resistance test methodology based on the unloading compliance (UC) procedure is introduced to provide the requisite background to determine fracture resistance data for these fracture specimens. A rather comprehensive presentation of the estimation formulas to evaluate *J* (and, equivalently, CTOD) and crack length from load-displacement (CMOD) records is also given. Constraint effects in SE(B) and clamped SE(T) specimens in terms of the $J-Q$ methodology are then described, followed by the presentation of key results for crack growth resistance testing conducted on low constraint fracture specimens extracted from typical pipe girth welds.

1. Introduction

Conventional testing programs to measure crack growth resistance curves routinely employ three-point bend, SE(B), or compact, C(T), specimens containing deep, through cracks ($a/W \geqslant 0.45 \sim 0.5$) - see Refs. [1,2] for further discussion. The key motivation to use deeply cracked specimens is to guarantee conditions leading to high crack-tip constraint with limited-scale plasticity. For these specimens, the near-tip region of elastic unloading and non-proportional loading is well contained within the *J*-dominance zone (i.e., the characteristic size of the region over which *J* provides a good description of the evolving stress and strain crack-tip fields) [3]. While such high triaxiality conditions prevail, there is a mechanistic rationale which supports predictive approaches to analyze crack extension and crack instability using crack resistance data based on experimentally measured *R*-curves. To insure stable crack growth under *J*-controlled conditions, testing standards for resistance curves (such as ASTM E1820 [4]) impose limits on the crack tip deformation relative to crack length, specimen thickness and remaining crack ligament. These limits are generally cast in the form of a size requirement expressed as $J_{max} = b\sigma_f/M$, where M represents the nondimensional deformation limit and $b = W - a$ denotes the uncracked ligament length in which W is the specimen width and a defines the crack size. Here, σ_f characterizes an effective yield strength for the tested material which is most often defined as $\sigma_f = (\sigma_{ys} + \sigma_{uts})/2$, where σ_{ys} is conveniently assigned the 0.2% offset yield stress and σ_{uts} is the ultimate tensile strength.

However, laboratory testing of fracture specimens to measure resistance curves consistently reveals a marked effect of absolute specimen size, geometry, relative crack size (a/W) and loading mode (tension vs. bending) on *R*-curves (see Refs. [5–7] for representative experimental studies). For the same material, deeply-notched SE(B) and C(T) specimens yield low *R*-curves while shallow-notch SE(B), single-edge notch tension, SE(T), and middle-crack tension, M(T), specimens yield larger toughness values at similar amounts of crack growth. These effects observed in *R*-curves have enormous practical implications in defect assessments and repair decisions of in-service structures under low constraint conditions thereby prompting research efforts to support the use of geometry dependent fracture toughness values in defect assessment procedures for specific structures, including pipeline girth welds. In fracture mechanics spirit, a predictive application of crack resistance data measured using low constraint fracture specimens to structural crack configurations of similar stress triaxiality potentially reduces the excessive conservatism that would otherwise arise in conventional defect assessments based on toughness data measured using high constraint fracture specimens. In

E-mail address: claudio.ruggieri@usp.br.

http://dx.doi.org/10.1016/j.ijpvp.2017.07.003
0308-0161/

particular, there has recently been a surge of interest in testing and standardizing single edge notch tension specimens (often termed SE(T) or SENT specimen geometries) to measure experimental *R*-curves more applicable to high pressure piping systems and pipe girth welds subjected to large strains [8–14]. Paralleling these efforts, another low constraint fracture specimen gaining increased attention is the shallow-crack bend specimen with $a/W \geqslant 0.2 \sim 0.25$. While perhaps slightly more conservative, testing of this specimen geometry may also become attractive due to its simpler and verified testing protocol, laboratory procedures and much smaller loads required to propagate the crack. Although deeply-cracked SE(B) specimens are the preferred crack geometry often adopted in conventional defect assessment methods, recent revisions of ASTM 1820 [4] and ISO 15653 [15] have also included *J*-estimation equations applicable to shallow-crack bend specimens.

The development of analytical and experimental procedures to measure the crack growth response in ductile materials has seen continuous progress since the pioneering work of Begley and Landes [16] who brought the energy release rate interpretation of the *J*-integral to bear on a laboratory testing method to characterize the critical value of *J* at the onset of ductile tearing using multiple fracture specimens with different crack lengths. Subsequently, Rice et al. [17] were the first to consider an alternative method to estimate *J* from a single measurement of load-displacement records which led to a substantial broadening of test procedures to evaluate fracture toughness for common specimen geometries. The introduction of a single specimen technique to estimate *J* and, later, an elastic unloading compliance approach proposed by Clark [18] to evaluate the amount of stable crack extension with increased loading provided the basis for generalizing the concept of *J*-resistance curves to characterize ductile tearing behavior under *J*-dominance conditions [3]. More recent efforts in this area have focused on the development of testing protocols for fracture resistance measurements in ductile materials using predominantly high constraint, deeply-cracked fracture specimens, such as the C(T) geometry, to guarantee conditions leading to *J*-controlled crack growth. Undoubtedly, the most widely representative and extensive test method practices for fracture toughness measurements, including the necessary analytical framework, have been put together in the form of ASTM E1820 [4] - see also the comprehensive review of Zhu and Joyce [19] and references therein. While valid objections might be raised to the actual significance of the use of deeply-cracked fracture specimens, fracture toughness data measured using ASTM E1820 [4] are expected to provide generally conservative structural integrity predictions of low constraint structural components containing crack-like flaws.

However, the technological importance of assessing the fracture behavior of cracked components under low constraint conditions has stimulated renewed interest in developing and testing specimen configurations which produce geometry and loading dependent fracture toughness measurements, including fracture resistance data. A case of considerable relevance includes structural defects in pressurized piping systems which are very often surface cracks that form during fabrication or during in-service operation (*e.g.*, blunt corrosion, slag and nonmetallic inclusions, weld cracks, dents at weld seams, etc. [20]). These crack configurations generally develop low levels of crack-tip stress triaxiality which contrast sharply to conditions present in deeply cracked specimens [21,22]. Consequently, predictions of structural fracture resistance based on standard, deep notch specimens may be unduly conservative and overly pessimistic. While such conservatism represents an extra factor of safety, excessive pessimism in defect assessments can potentially have strong impact on flaw acceptance criteria and lead to unwarranted repairs or replacement of in-service pipelines at great operational costs.

The above arguments prompted fundamental investigations on low constraint geometries to support the use of single edge notch tension configurations, either under fixed grip or pin-loading conditions, in fracture assessment procedures more applicable to thin-walled pipes under bending having surface flaws - these studies include the representative works of Chiesa et al. [23] and Cravero and Ruggieri [21], among others. These early analyses have evolved into more specific procedures to evaluate crack growth resistance curves in ductile materials in which a consensus has emerged in favor of the use of clamped SE(T) specimens with a fixed clamp distance over specimen width ratio (H/W) of 10 as the preferred test configuration for generating geometry fracture toughness data based on load-crack mouth opening displacement (CMOD) records. The first attempt to produce a standardized SE(T) test procedure applicable to pipeline girth welds was made by Det Norske Veritas (DNV) [10] which adopted a multiple specimen technique to evaluate a *J*-resistance curve based on simplified equations incorporating the η-method [1,24–26] to experimentally determine *J*-values when the amount of the ductile crack growth is less than 10% of the initial remaining ligament $(W - a_0)$, with a_0 denoting the initial crack size. Following the DNV approach, a number of SE(T) test procedures for fracture resistance measurements in terms of $J - \Delta a$ or CTOD $-$ Δa data have been introduced, most adopt a single specimen technique using the unloading compliance (UC) method to estimate the amount of stable crack growth. These research efforts include the previous studies of Cravero and Ruggieri [27,28] and Shen et al. [13,14,29,30]. These workers gave a representative set of η-factors and compliance solutions for evaluating *J* and Δa to support accurate measurements of fracture resistance curves. Subsequently, ExxonMobil [12], Pussegoda et al. [8] and Verstraete et al. [31] extended the latter methodologies to introduce relatively more comprehensive SE(T) test procedures to experimentally evaluate fracture resistance data in terms of CTOD resistance curves in which the CTOD is derived from the double clip-gage technique [32,33]. The British Standards Institution has recently published a new standard in the form of BS 8571 [9] providing the essential methodology to determine fracture resistance in metallic materials mainly in terms of CTOD $-$ *R* curves (the standard adopts the same formulations to evaluate *J* derived from the DNV procedure [10]). A number of important applications of these procedures have been made to measure fracture resistance in ductile materials, including those reported by Mathias et al. [7], Park et al. [34], Verstraete et al. [35], Zhu et al. [36] and Sarzosa et al. [33]. Moreover, a recent round robin test program [37] conducted under a Pipeline Research Council International (PRCI) project provided further support to the standardization of the SE(T) test methodology in fracture resistance measurements applicable to pipeline girth welds. Zhu and McGaughy [38] and Zhu [39] provide a brief survey of these fracture resistance test methods using SE(T) specimens.

In spite of the promise evident in these works, some difficulties associated with SE(T) testing procedures, including fixture and gripping conditions, raise potential concerns about the significance and qualification of measured crack growth resistance curves. For example, it has been reported some tendency for developing uneven crack advance and a rather irregular crack front profile in tested SE(T) specimens, even for side-grooved configurations, which can most likely be attributed to the strong tensile mode fields and associated large plastic strains developing at the specimen free surfaces - this, in turn, can lead to large differences between UC predictions of crack extension and measured post test crack growth (see illustrative example by Drexler et al. [40]) thereby potentially affecting the specification of tolerable defect sizes. In contrast, while perhaps slightly more conservative, testing of shallow-crack bend specimens configuration has emerged as a

viable alternative. In retrospect, only a limited number of studies have examined the applicability of shallow-crack SE(B) geometries to fracture resistance measurements of ductile materials and, more particularly, pipeline girth welds, including those of Park et al. [41] and Mathias et al. [7]. Nevertheless, the fracture test procedures that are already in place for this specimen configuration lend strong support to more actively pursue further developments of shallow-crack bend specimen techniques to generate fracture resistance curves for pipeline welds.

This work presents a brief review of current progress in fracture resistance test procedures to measure crack growth properties of pipeline steels using clamped SE(T) and shallow-crack SE(B) specimens. A central objective is to assess recently developed practices for J and CTOD resistance curve test methods with particular emphasis on the estimation procedures for J and CTOD as well as the experimental evaluation of stable crack growth. The plan of the paper is as follows. The next section introduces an overview of the fracture resistance test methodology based on the unloading compliance (UC) procedure and provides the requisite background to determine fracture resistance data for common fracture specimens, including low constraint geometries. A rather comprehensive presentation of the estimation formulas to evaluate J (and, equivalently, CTOD) and crack length from load-displacement (CMOD) records is also given. Constraint effects in SE(B) and clamped SE(T) specimens in terms of the $J-Q$ methodology are then described, followed by the presentation of key results of crack growth resistance testing conducted on low constraint fracture specimens extracted from typical pipe girth welds. A short discussion on the effectiveness of the UC procedure using low constraint fracture specimens to characterize stable crack growth in ductile materials concludes this paper.

2. Overview of fracture resistance test methodology

This section briefly addresses the essential features of the analytical framework that have a direct bearing on the evaluation procedure of fracture resistance curves for common fracture specimens, including the clamped SE(T) and SE(B) configurations, from laboratory measurements of load-displacement records. Implementation of the methodology essentially follows conventional procedures based on the unloading compliance (UC) technique using a single specimen test to determine the instantaneous value of the specimen compliance at partial unloading during the measurement of the load *vs.* displacement curve thereby enabling accurate estimations of J (or δ) and Δa at several locations on the load-displacement records from which the $J-R$ and $\delta-R$ curves can be developed. Readers are referred to the works of Joyce [2], Cravero and Ruggieri [27,28], Mathias et al. [7], Zhu and Joyce [19], Zhu [38] and references therein for a more complete discussion of the evaluation method for crack growth resistance curves.

2.1. Evaluation procedure of J

For the purpose of developing the framework to evaluate the crack driving force, as characterized by the J-integral, with increased amounts of stable crack growth, it is helpful to consider an incremental procedure which updates J in terms of its elastic component, J_e, and plastic component, J_p, at each partial unloading point, denoted k, during the measurement of the load vs. displacement curve illustrated in Fig. 1(a) as

$$J^k = J_e^k + J_p^k \tag{1}$$

where the current elastic term is given by

$$J_e^k = \left(\frac{K_I^2}{E'}\right)_k \tag{2}$$

in which K_I is the elastic stress intensity factor for the cracked configuration at the k-th unloading point and $E' = E/(1-\nu^2)$, where E and ν are the (longitudinal) elastic modulus and Poisson's ratio, respectively. For the SE(T) and SE(B) geometries discussed here, solutions for K_I can be found in several previously published works, such as Tada et al. [42] and Cravero and Ruggieri [27] among others.

Now, directing attention to the evaluation of the plastic term, J_p^k, early methods to measure J-resistance curves adopted an incremental equation to estimate J_p based entirely on load-load line displacement (LLD) records which derives from the fundamental work of Ernst et al. [43]. However, when the crack growth response is measured in terms of load-crack mouth opening displacement (CMOD) records, Cravero and Ruggieri [28] and Zhu et al. [44] introduced an incremental formulation to determine J_p in the form

$$J_p^k = \left[J_p^{k-1} + \frac{\eta_{J-CMOD}^{k-1}}{b_{k-1}B_N}\left(A_p^k - A_p^{k-1}\right)\right]\cdot\Gamma_k \tag{3}$$

with Γ_k defined by

$$\Gamma_k = \left[1 - \frac{\gamma_{LLD}^{k-1}}{b_{k-1}}(a_k - a_{k-1})\right] \tag{4}$$

where factor γ_{LLD} is evaluated from

$$\gamma_{LLD} = \left[-1 + \eta_{J-LLD}^{k-1} - \left(\frac{b_{k-1}}{W\eta_{J-LLD}^{k-1}}\frac{d\eta_{J-LLD}^{k-1}}{d(a/W)}\right)\right] \quad , \tag{5}$$

where it is noted that all quantities entering into Eqs. (3)–(5) are referred to the k-th unloading point in view of the adopted incremental procedure. Further, A_p represents the plastic area under the load-displacement curve, B_N is the net specimen thickness at the side groove roots ($B_N = B$ if the specimen has no side grooves where B is the specimen gross thickness), a is the crack length, b denotes the uncracked ligament ($b = W - a$ where W is the width of the cracked configuration and a is the crack length).

In the above, factor η represents a nondimensional parameter which relates the plastic contribution to the strain energy for the cracked body with J. It is also noted that A_p (and consequently, η_J) can be defined in terms of load-load line displacement (LLD or Δ) data or load-crack mouth opening displacement (CMOD or V) data and, thus, the corresponding quantities are referred to as η_{J-LLD} and η_{J-CMOD} in the present article. Moreover, it is also noted that the incremental formulation to determine J_p given by Eq. (3) incorporates an additional term, represented by Γ_k, to correct the measured load-displacement records for crack extension (see Anderson [1], Kanninen and Popelar [24] and Cravero and Ruggieri [28]). Here, further observe that the crack resistance evaluation procedure does not require any displacement measurements other than CMOD as the quantity Γ_k is associated with an available solution for η_{J-LLD} and not with LLD measurements.

2.2. Crack extension measurements

The accurate measurement of the specimen compliance evaluated at periodic unloadings with increased deformation is a key step in the UC procedure to obtain highly precise estimates of the (current) crack length, a_k, which are, in turn, highly descriptive of

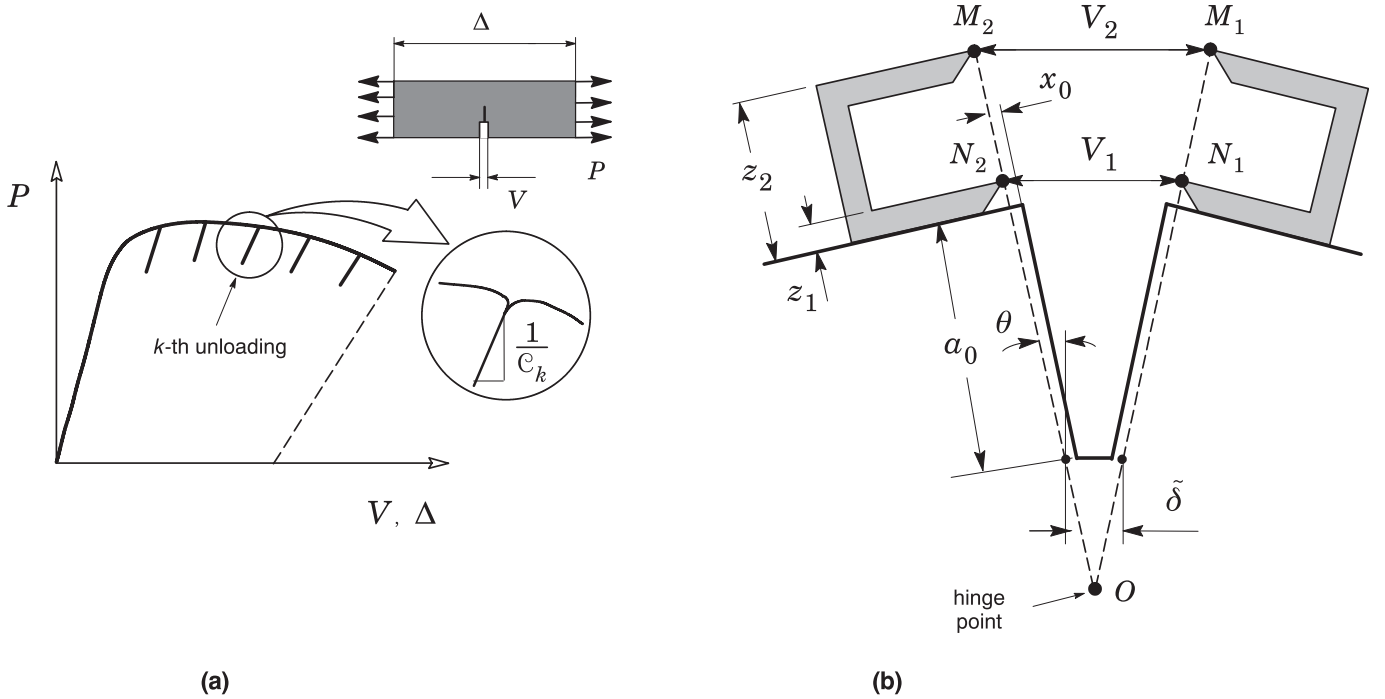

Fig. 1. (a) Simplified scheme of the incremental methodology to evaluate J based on the plastic area under the load-displacement (CMOD or V) curve using the UC procedure. (b) Double clip-gage method to estimate the CTOD using measurements of crack opening displacements (COD) at two different points.

the physical amount of stable crack growth. Moreover, as indicated in the above Eqs. (3)–(5), the accurate crack length estimation affects directly the accuracy of the J-integral update during the incremental procedure.

The slope of the load-displacement curve during the $k-th$ unloading illustrated in Fig. 1(a) defines the current specimen compliance, denoted C_k, which depends on specimen geometry and crack length. For the specimen geometries under consideration here, the specimen compliance based on CMOD is most often defined in terms of normalized quantities expressed as

$$\mu_{CMOD}^{SET} = \left[1 + \sqrt{EB_eC_{CMOD}}\right]^{-1} \tag{6}$$

$$\mu_{CMOD}^{SEB} = \left[1 + \sqrt{\frac{EWB_eC_{CMOD}}{S/4}}\right]^{-1} \tag{7}$$

where μ_{CMOD}^{SET} and μ_{CMOD}^{SEB} define the normalized compliances for the SE(T) and SE(B) specimens. In the above expressions, C_{CMOD} denotes the specimen compliance defined in terms of crack mouth opening displacement ($C = V/P$ where V is the CMOD and P represents the applied load) and the effective thickness, B_e, is defined by

$$B_e = B - \frac{(B - B_N)^2}{B} \tag{8}$$

2.3. Evaluation procedure of CTOD

To the extent that J describes the crack-tip conditions with increased crack extension and, further, that a unique $J-$CTOD relationship holds true for stationary and growing cracks, both $J-R$ and CTOD $-R$ curves equally characterize well the crack growth resistance behavior for the tested material [1,3]. Thus, the same analysis as above may be followed when the CTOD (δ) is adopted to characterize the crack-tip driving force. Since, under conditions of large-scale yielding, a relation between J and CTOD is expressed in the form [1,19,32,45,46]

$$\delta = \frac{J}{m\sigma_0}, \tag{9}$$

the CTOD can be advantageously determined by evaluating J using the plastic work defined by the area under the load vs. CMOD curve and then converting it into the corresponding value of CTOD - observe that Eq. (9) relates the total value of the experimentally measured J to the total value of CTOD. The approach has the potential to simplify evaluation of CTOD values while, at the same time, relying on a rigorous energy release rate definition of J for a cracked body. In the above, m represents a proportionality coefficient strongly dependent on the material strain hardening but weakly sensitive to crack size as characterized by the a/W-ratio and σ_0 defines a reference stress value, usually taken as the material yield stress, σ_{ys}, or the flow stress, σ_f. Here, most CTOD evaluation procedures, including ASTM 1820 [4] and the expressions provided later in Section 3.3, adopt the flow stress, σ_f, to define the $J-$CTOD relationship and, consequently, parameter m entering into previous Eq. (9).

While the previous methodology has proven effective in routine procedures to evaluate the CTOD, it does require the determination of J and the knowledge of accurate values for the η-factor and parameter m. To provide a simpler extension of the plastic hinge concept applicable to broader crack configurations, a double clip-gage arrangement can also be used as an alternative method to estimate the CTOD from adequate measurements of crack opening displacements (COD) at two different points. Fig. 1(b) schematically illustrates the essential features of the procedure in which a pair of knife edges is attached on each side of the notch close to the notch mouth to allow the use of two clip-gages to measure the displacement at these knife edge positions - such double clip-gage

(DCG) fixture is currently recommended by recent test procedures to evaluate resistance curves using clamped SE(T) specimens [8,9,12]. With the method illustrated in Fig. 1(b), a simple geometrical approach then enables defining the CTOD (δ) in terms of the two measured COD-values. Here, the double clip-gage arrangement shown in Fig. 1(b) deserves attention since the DCG mounting fixture is typically installed at a distance x_0 from the notch flank as shown in 1(b); only when $x_0 = 0$ can the DCG fixture be considered aligned with the specimen machined notch and the fatigue precrack. This practice results in an *apparent* offset of the crack flank thereby potentially increasing the measured CTOD, here denoted as $\tilde{\delta}$ in the figure. The specification of x_0 in the test protocol introduces an explicit dimension in the test procedure and opens the possibility to correct the measured CTOD $-$ R curve for different values of x_0. However, this option was not examined in the present work so that hereafter we refer to $\tilde{\delta}$ as δ for simplicity. Moreover, the DCG procedure implies a rigid rotation of the crack flank defined from the crack mouth to the crack tip, which may represent another possible cause for the apparent increase in experimentally measured CTOD-values. The proper evaluation of the CTOD based on the DCG procedure remains an open issue and an investigation along this line is in progress.

Now, by measuring two COD-values, V_1 and V_2, at two locations on a straight line passing through the crack flank of the specimen and assuming rigid body rotation, then a geometrical relationship between the CTOD (δ) and both measured COD-values is obtained in the form

$$\delta = V_1 - \frac{z_1 + a_0}{z_2 - z_1}(V_2 - V_1) \tag{10}$$

where z_1 and z_2 represent the distance of the measuring points for V_1 and V_2 from the specimen surface as depicted in Fig. 1(b). Here, it is noted that the crack size, a_0, entering into Eq. (10) represents the initial crack length not the current crack size measured at the extending tip as discussed by Sarzosa et al. [32]. Moreover, also observe that the CTOD is defined here as the crack opening at the position of the original crack tip such that, with crack-tip blunting, the position of the original crack tip falls slightly behind the current crack tip.

3. Recent estimation formulas for crack growth resistance curves

Evaluation of crack growth resistance curves from load-displacement records using the UC procedure outlined above requires the specification of the key quantities defining J and Δa, including the plastic η-factors appearing in Eqs. (3) and (5) as well the specimen compliance entering into Eqs. (6) and (7). A number of somewhat different expressions describing these quantities have been obtained through several recent efforts in this area in connection with the development of experimental procedures to evaluate fracture resistance data for ductile materials, most of them derived from finite element analysis of selected fracture specimens. This section provides a relatively broad summary of the estimation formulas for crack growth resistance curves derived from previously published solutions for plastic η-factors, specimen compliance and $J-$CTOD relationships applicable to the 3P SE(B) specimens and clamped SE(T) geometries shown in Fig. 2.

3.1. Numerical solutions for plastic η factors

All the expressions for the plastic η-factors presented in this section are for elastic-plastic materials obeying a simple power-hardening model to characterize the uniaxial true stress ($\overline{\sigma}$) *vs.* logarithmic strain ($\overline{\varepsilon}$) in the form $\overline{\varepsilon}/\varepsilon_{ys} \propto (\overline{\sigma}/\sigma_{ys})^n$, where ε_{ys} is the

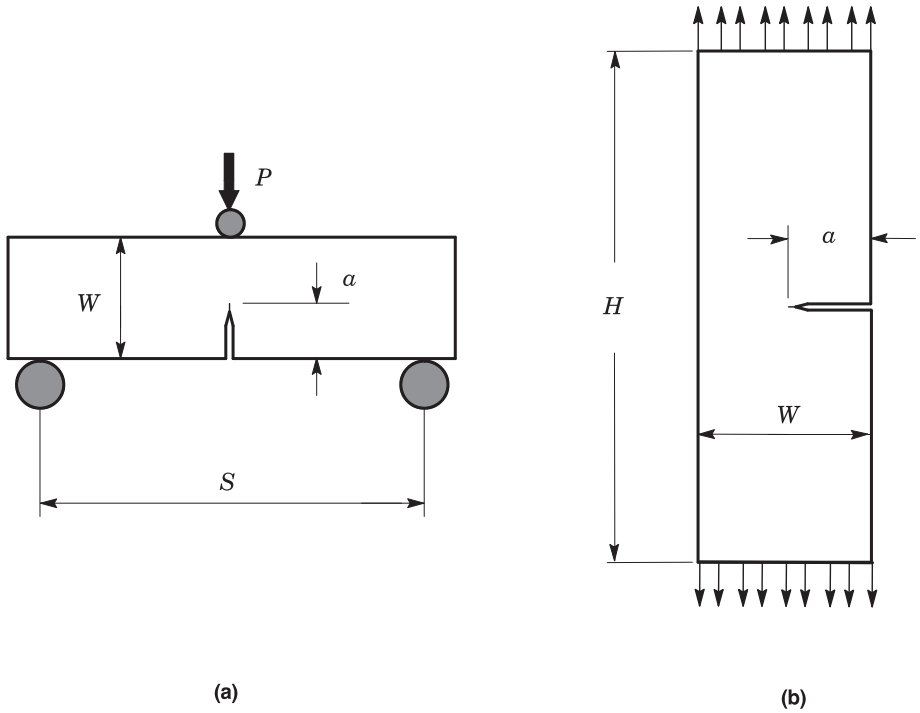

Fig. 2. Bending and tensile-loaded geometries considered in the present study: (a) 3-point SE(B) specimen. (b) Single edge notch tension SE(T) specimen with fixed-grip loading (clamped ends).

yield strain and n is the Ramberg-Osgood strain hardening exponent [1]. Here, because the plastic η-factors based on CMOD are essentially insensitive to strain hardening behavior (see, *e.g.,* Kirk and Dodds (K&D) [45] and other studies described below), the numerical solutions for factors η_{J-CMOD} described below are valid for any value of n. In contrast, the numerical solutions for factors η_{J-LLD} do exhibit a somewhat stronger dependence on n, particularly for shorter crack sizes. Observe, however, that η_{J-LLD} is only used to determine Γ_k, which, in turn, is employed to correct the measured load-displacement records for crack extension (refer to Section 2.1). Since the crack growth correction term is usually relatively small ($\approx 10 \sim 20\,\%$) - (see Mathias et al. [7] for illustrative results), the expressions for factors η_{J-LLD} presented here correspond to average values and are therefore considered applicable to any value of n.

3.1.1. SE(B) specimens

By using nonlinear finite element analyses for plane-strain models of SE(B) fracture specimens, previous investigations have introduced slightly different expressions describing the plastic η-factor based on CMOD for this specimen configuration. These expressions are described below and displayed in Fig. 3(a) to aid in assessing the relative differences.

- Kirk and Dodds (K&D) [45]

$$\eta^{SEB}_{J-CMOD} = 3.785 - 3.101\left(\frac{a}{W}\right) + 2.018\left(\frac{a}{W}\right)^2, \quad 0.05 \le a/W \le 0.7 \tag{11}$$

- Kim and Schwalbe (K&S) [47]

$$\eta^{SEB}_{J-CMOD} = 3.724 - 2.244\left(\frac{a}{W}\right) + 0.408\left(\frac{a}{W}\right)^2, \quad 0.05 \le a/W \le 0.7 \tag{12}$$

- Donato and Ruggieri (D&R) [48]

$$\eta^{SEB}_{J-CMOD} = 3.650 - 2.111\left(\frac{a}{W}\right) + 0.341\left(\frac{a}{W}\right)^2, \quad 0.15 \le a/W \le 0.7 \tag{13}$$

- Zhu et al. [44]

$$\eta^{SEB}_{J-CMOD} = 3.667 - 2.199\left(\frac{a}{W}\right) + 0.437\left(\frac{a}{W}\right)^2, \quad 0.05 \le a/W \le 0.7 \tag{14}$$

- Souza and Ruggieri (S&R) [49] (Plane-strain analysis)

$$\eta^{SEB}_{J-CMOD} = 3.432 - 1.647\left(\frac{a}{W}\right) + 0.065\left(\frac{a}{W}\right)^2, \quad 0.1 \le a/W \le 0.7 \tag{15}$$

- Souza and Ruggieri (S&R) [49] (3-D analysis)

$$\eta^{SEB}_{J-CMOD} = 3.862 - 3.550\left(\frac{a}{W}\right) + 1.659\left(\frac{a}{W}\right)^2, \quad 0.1 \le a/W \le 0.7 \tag{16}$$

The resulting expression proposed by Zhu et al. [44] is actually a 2-nd order polynomial fit to available plane-strain results for η_{J-CMOD}, including those from Kirk and Dodds [45], Kim and Schwalbe [47] and Donato and Ruggieri [48], and is currently adopted by ASTM E1820 [4], ASTM E1921 [50] and ISO 15653 [15]. A closer examination of the results displayed in Fig. 3(a) reveals that the numerical η-values obtained by Zhu et al. [44] are virtually indistinguishable from the numerical expressions derived from Kim and Schwalbe [47] and Donato and Ruggieri [48]. By contrast, the numerical results reported by Kirk and Dodds [45] and Souza and Ruggieri [49] exhibit some differences in the computed η-values compared to the results of Zhu et al. [44], although these are confined to the early and late part of the curve; in particular, the η-values obtained by Kirk and Dodds [45] are slightly nonconservative for deeply cracked bend specimens. Moreover, the previous η-factor equations reflect the effect of strain energy for the cracked body, described by the plastic work associated with the load-CMOD curve, on the applied J derived from plane-strain analyses of conventional SE(B) specimens. In related work, Nevalainen and Dodds [51] examined the through-thickness dependence of the crack front fields in 3-D models of SE(B) configurations to find a coupling effect of a/W and W/B ratios with material hardening properties on fracture behavior. These observations motivated Souza and Ruggieri [49] to conduct rather extensive finite element analyses on 3-D models of plane-sided and side-grooved SE(B) specimens. Their

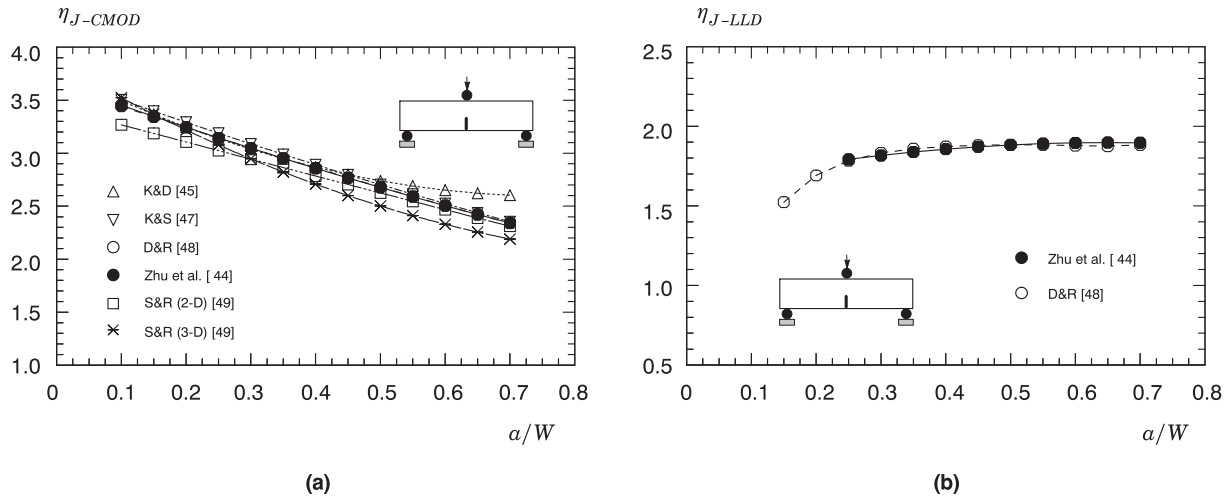

Fig. 3. Dependence of plastic factor η_J on a/W for standard 3P SE(B) specimens: (a) η_J based on CMOD. (a) η_J based on LLD.

3-D analyses demonstrate a relatively weak effect of out-of-plane constraint associated with specimen thickness on factors η_{J-CMOD}. To facilitate the comparison with plane-strain results, Fig. 3(a) also includes the 3-D results from Souza and Ruggieri [49]. While the computed 3-D η_{J-CMOD} factors are lower than the corresponding plane-strain values in the late part of curve, they are nevertheless fairly close to the expression obtained by Zhu et al. [44].

As outlined in Section 2, when the incremental estimation procedure for J includes the effects of crack growth on plastic work, the incremental expression for J_p defined by Eq. (3) contains an additional contribution due to crack growth correction in terms of LLD by means of factor η_{J-LLD}. Two widely used expressions are given below and shown in Fig. 3(b). The present solution for η_{J-LLD} from Donato and Ruggieri [48], which was also adopted in recent work by Mathias et al. [7], represents a more convenient 5th-order polynomial fit to their original results. The agreement between the η_{J-LLD} -values from these expressions for $a/W \geq 0.25$ is evident in this plot. In particular, the η_{J-LLD} equation derived from Zhu et al. [44] is also incorporated into ASTM E1820 [4] through the factor γ_{LLD} defined in previous Eq. (5).

- Donato and Ruggieri (D&R) [48]

$$\eta_{J-LLD}^{SEB} = 0.020 + 18.086\frac{a}{W} - 73.246\left(\frac{a}{W}\right)^2 + 152.225\left(\frac{a}{W}\right)^3 - \\ -159.769\left(\frac{a}{W}\right)^4 + 66.879\left(\frac{a}{W}\right)^5, \quad 0.15 \leq a/W \leq 0.7 \tag{17}$$

- Zhu et al. [44]

$$\eta_{J-LLD}^{SEB} = \left[0.436 + 0.534\left(\frac{a}{W}\right)\right]\left[3.667 - 2.199\left(\frac{a}{W}\right) + 0.437\left(\frac{a}{W}\right)^2\right], \\ 0.25 \leq a/W \leq 0.7 \tag{18}$$

The trends displayed in Fig. 3(a–b) provide strong support for using the η-factor solutions given by ASTM E1820 [4] in fracture toughness measurements of metallic materials utilizing standard SE(B) specimens. Apart from small differences in η-values in comparison with other solutions, the η_J expressions presented in current version of ASTM E1820 [4] provide accurate estimates of J for both shallow and deep crack fracture toughness testing for materials with a wide range of strain hardening properties.

3.1.2. Clamped SE(T) specimens

While there has been rather extensive work on developing improved expressions for plastic η-factors applicable to conventional fracture specimens, including the SE(B) geometry previously described, only relatively limited studies [5,10,13,25–27,52] have developed wide range J estimation equations for SE(T) geometries with $H/W = 10$ based on η-factors. Most of them, including the works of Joyce et al. [5], Cravero and Ruggieri (C&R) [27], Ruggieri [25] and Paredes and Ruggieri [26], focused on developing η-factor solutions in a 2-D, plane-strain setting whereas DNV F108 [10], Shen and Tyson (S&T) [13] and Wang et al. [52] provide expressions for the plastic η-factors in a 3-D setting. In particular, Wang et al. [52] conducted extensive 3-D finite element analyses on clamped SE(T) models with varying B/W-ratios which led to a relatively broader set of η-factor solutions explicitly incorporating the effects of specimen thickness. The resulting fitting equations describing the plastic η-factors introduced by Wang et al. [52] are unfortunately a little complex to implement in general but their study suggests a potential dependence of factor η on the B/W-ratio for this specimen geometry; however, the actual effect on the measured crack growth resistance curve remains untested. Thus, the present paper favors simpler expressions describing the plastic η-factors, which are listed below and shown in Fig. 4(a–b) to facilitate comparisons.

- DNV F108 [10] ($B/W = 1$)

$$\eta_{J-CMOD}^{SET} = 0.238 + 8.478\frac{a}{W} - 33.769\left(\frac{a}{W}\right)^2 + 54.660\left(\frac{a}{W}\right)^3 - 36.308\left(\frac{a}{W}\right)^4 + 6.568\left(\frac{a}{W}\right)^5, \quad 0.2 \leq a/W \leq 0.5 \tag{19}$$

- Cravero and Ruggieri (C&R) [27]

$$\eta_{J-CMOD}^{SET} = 1.040 - 0.687\left(\frac{a}{W}\right), \quad 0.1 \leq a/W \leq 0.7 \tag{20}$$

- Shen and Tyson (S&T) [13]

$$\eta_{J-CMOD}^{SET} = 1 - 1.089\left(\frac{a}{W}\right) + 9.519\left(\frac{a}{W}\right)^2 - 48.572\left(\frac{a}{W}\right)^3 + 109.225\left(\frac{a}{W}\right)^4 - \\ -73.116\left(\frac{a}{W}\right)^5 - 77.984\left(\frac{a}{W}\right)^6 + 38.487\left(\frac{a}{W}\right)^7 + 101.401\left(\frac{a}{W}\right)^8 + \\ +43.306\left(\frac{a}{W}\right)^9 - 110.770\left(\frac{a}{W}\right)^{10}, \quad 0.1 \leq a/W \leq 0.7 \tag{21}$$

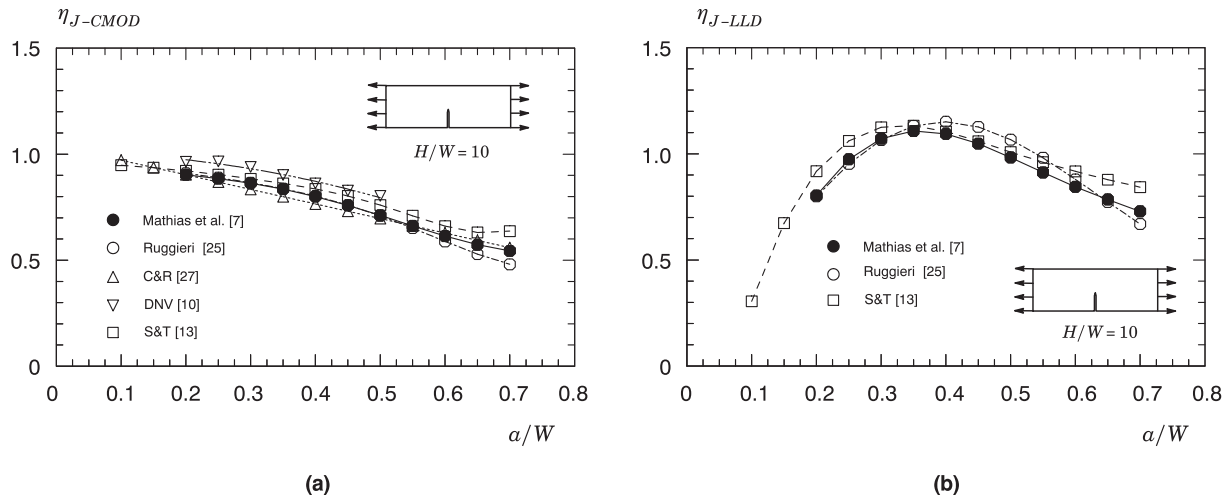

Fig. 4. Variation of plastic factor η_J with a/W for clamped SE(T) specimens with $H/W = 10$: (a) η_J based on CMOD. (a) η_J based on LLD.

$$\eta^{SET}_{J-LLD} = -0.880 + 15.190\left(\frac{a}{W}\right) - 35.440\left(\frac{a}{W}\right)^2 + 18.644\left(\frac{a}{W}\right)^3 + 18.399\left(\frac{a}{W}\right)^4 - \\ -1.273\left(\frac{a}{W}\right)^5 - -12.756\left(\frac{a}{W}\right)^6 - 12.202\left(\frac{a}{W}\right)^7 - 4.447\left(\frac{a}{W}\right)^8 + \\ +5.397\left(\frac{a}{W}\right)^9 + 14.187\left(\frac{a}{W}\right)^{10}, \quad 0.1 \le a/W \le 0.7 \tag{22}$$

- Ruggieri [25]

$$\eta^{SET}_{J-CMOD} = 0.972 - 0.028\frac{a}{W} - 3.028\left(\frac{a}{W}\right)^2 + 12.398\left(\frac{a}{W}\right)^3 - \\ -24.577\left(\frac{a}{W}\right)^4 + 15.829\left(\frac{a}{W}\right)^5, \quad 0.2 \le a/W \le 0.7 \tag{23}$$

$$\eta^{SET}_{J-LLD} = 0.222 + 0.287\frac{a}{W} + 26.774\left(\frac{a}{W}\right)^2 - 86.565\left(\frac{a}{W}\right)^3 + \\ +95.246\left(\frac{a}{W}\right)^4 - 35.999\left(\frac{a}{W}\right)^5, \quad 0.2 \le a/W \le 0.7 \tag{24}$$

- Mathias et al. [7]

$$\eta^{SET}_{J-CMOD} = 1.067 - 1.767\frac{a}{W} + 7.808\left(\frac{a}{W}\right)^2 - 18.269\left(\frac{a}{W}\right)^3 + \\ +15.295\left(\frac{a}{W}\right)^4 - 3.083\left(\frac{a}{W}\right)^5, \quad 0.2 \le a/W \le 0.7 \tag{25}$$

$$\eta^{SET}_{J-LLD} = -0.623 + 9.336\frac{a}{W} - 4.584\left(\frac{a}{W}\right)^2 - 47.963\left(\frac{a}{W}\right)^3 + \\ +87.697\left(\frac{a}{W}\right)^4 - 44.875\left(\frac{a}{W}\right)^5, \quad 0.2 \le a/W \le 0.7 \tag{26}$$

All the results displayed in Fig. 4(a–b) have the common feature of having similar variation of factor η_J with crack size as characterized by the a/W-ratio. Further, the present solutions for η_{J-CMOD} and η_{J-LLD} from Ruggieri [25] are derived from a more convenient 5th-order polynomial fit to those original results for the purpose of providing simpler and yet broader expressions describing factor η_J . Consider first the η_{J-CMOD} results shown in Fig. 4(a). The significant features include: (1) there is relatively good agreement for all expressions describing factor η_{J-CMOD} , particularly in the range $0.2 \le a/W \le 0.6$; (2) the DNV expression used in the present comparisons (which is applicable for specimen geometries having $B/W = 1$) provides the largest η_{J-CMOD}-values for a given a/W-ratio and is thus nonconservative (*i.e.*, it leads to higher *J*-resistance curves), and (3) the Shen and Tyson [13] expression also provides slightest larger η_{J-CMOD}-values for a given a/W-ratio in comparison to the results of Ruggieri [25] and Mathias et al. [7] but which are, nevertheless, in the difference range of $\sim 5\%$ for $0.3 \le a/W \le 0.6$. Consider next the η_{J-LLD} results shown in Fig. 4(b). These trends remain largely unchanged in which there is relatively good agreement for all expressions describing factor η_{J-LLD} . Observe that Shen and Tyson [13] expression does provide larger η_{J-LLD}-values for $a/W \ge 0.5$; such differences, however, should not cause major concerns since the crack growth contribution to J_p defined in Eq. (3) is expected to be small. Overall, the previous results seem to slightly favor the use of the η-factor solutions given by Ruggieri [25] as they have been validated by further analyses based on the load separation method and a numerical framework for *J* evaluation procedure using multispecimen measurements.

3.2. Crack length derived from elastic compliance solutions

3.2.1. SE(B) specimens

Previous fracture resistance test procedures using 3P SE(B)

specimens often adopted the relationship between load and CMOD derived from the elastic solution provided by Tada et al. [42] to arrive at a functional dependence of crack length and specimen compliance which provides accurate estimates of crack length for the unloading compliance method [5,53]. More recent developments in fracture toughness test procedures favor the use of elastic compliance solutions (from which the relationship between crack length and specimen compliance is derived) based on standard elastic, finite element analyses under plane-strain conditions to define the (linear) dependence of applied load on displacement with different crack length. Some of the most representative equations describing the variation of a/W with μ for the 3P SE(B) specimen are given below.

- Cravero [54]

$$\left(\frac{a}{W}\right)_{SEB} = 0.7590 + 1.2961\mu - 37.9076\mu^2 + 154.9671\mu^3 - 270.3815\mu^4 + +182.6632\mu^5, \quad 0.1 \le a/W \le 0.5 \tag{27}$$

- ASTM E1820 [4]

$$\left(\frac{a}{W}\right)_{SEB} = 1.0188 - 4.5367\mu + 9.0101\mu^2 - 27.3330\mu^3 + 74.4000\mu^4 - 71.4890\mu^5, \ 0.05 \le a/W \le 0.45 \tag{28}$$

$$\left(\frac{a}{W}\right)_{SEB} = 0.9997 - 3.9504\mu + 2.9821\mu^2 - 3.2141\mu^3 + 51.5156\mu^4 - 113.0310\mu^5, \ 0.45 < a/W \le 0.7 \tag{29}$$

- Souza and Ruggieri (S&R) [53]

$$\left(\frac{a}{W}\right)_{SEB} = 1.003 - 4.0437\mu + 4.7902\mu^2 - 13.7062\mu^3 + 59.6424\mu^4 - 71.7480\mu^5 \ , \ 0.1 \le a/W \le 0.8 \tag{30}$$

Fig. 5(a) compares the dependence of a/W with specimen compliance, μ, for the previous expressions. While the Cravero results [54] are slightly above the other results, the variation of a/W with μ given by ASTM E1820 [4] is virtually the same as the S&R [53] expression. However, it is of interest to note that ASTM E1820 actually provides two different expressions, one for shallow-cracks ($0.05 \le a/W \le 0.45$) and the other for deep cracks ($0.45 < a/W \le 0.7$), which may become somewhat cumbersome and potentially inaccurate when measuring, for example, the crack length in fracture specimens with moderate crack sizes ($a/W \approx 0.35 \sim 0.4$). Thus, these observations seem to favor the adoption of the S&R [53] expression in future revisions of ASTM E1820 test standard.

3.2.2. Clamped SE(T) specimens

Because of the nonstandard nature of this specimen, only few solutions describing the dependence of crack length and specimen compliance are available. These expressions are provided below and displayed in Fig. 5(b) to aid in assessing the relative differences.

- Cravero and Ruggieri (C&R) [27]

$$\left(\frac{a}{W}\right)_{SET} = 1.6485 - 9.1005\mu + 33.0250\mu^2 - 78.4670\mu^3 + 97.3440\mu^4 - 47.2270\mu^5, \quad 0.1 \le a/W \le 0.7 \tag{31}$$

- Mathias et al. [7]

$$\left(\frac{a}{W}\right)_{SET} = 1.9215 - 13.2195\mu + 58.7080\mu^2 - 155.2823\mu^3 + 207.3987\mu^4 - 107.9176\mu^5, \quad 0.1 \le a/W \le 0.7 \tag{32}$$

- Shen and Tyson (S&T) [13]

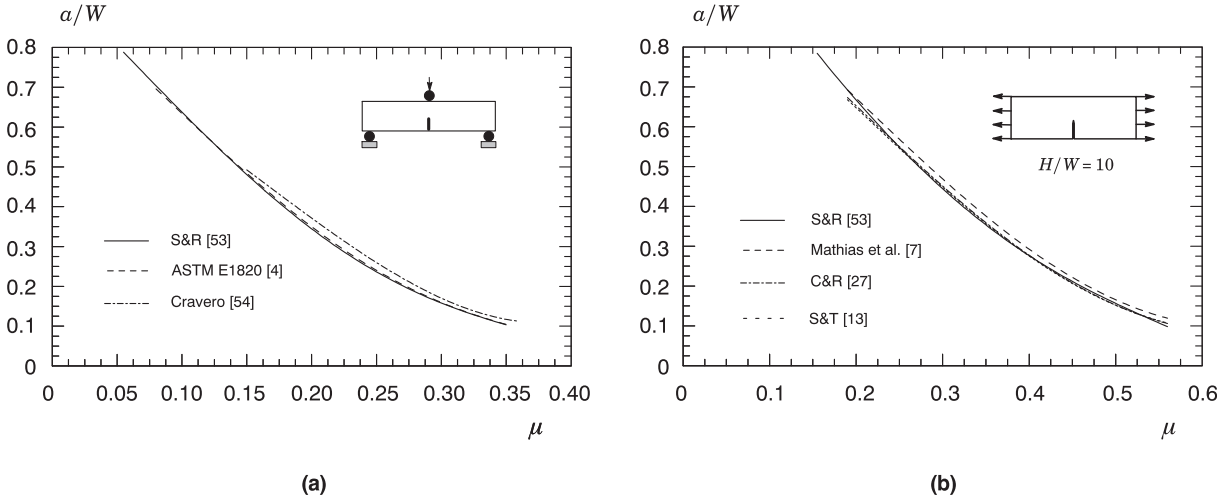

Fig. 5. Dependence of a/W on specimen compliance: (a) Standard 3P SE(B) specimens. (b) clamped SE(T) specimens with $H/W = 10$.

$$\left(\frac{a}{W}\right)_{SET} = 2.072 - 16.411\mu + 79.600\mu^2 - 211.670\mu^3 + 236.857\mu^4 + 27.371\mu^5 - 179.740\mu^6 - 86.280\mu^7 + 171.764\mu^8, \quad 0.1 \le a/W \le 0.7 \tag{33}$$

- Souza and Ruggieri (S&R) [53]

$$\left(\frac{a}{W}\right)_{SET} = 1.7548 - 10.7686\mu + 43.1621\mu^2 - 108.2553\mu^3 + 139.5816\mu^4 - 70.3533\mu^5, \quad 0.1 \le a/W \le 0.8 \tag{34}$$

Fig. 5(b) clearly shows the excellent agreement among these results, particularly for the C&R [27], S&T [13] and S&R [53] expressions. Observe that the results derived by Mathias et al. [7] are slightly more conservative since, for a given value of μ, their expression provides slightly larger crack length estimates. Further observe that the S&R [53] expression advantageously spans a wider range of crack size $(0.1 \le a/W \le 0.8)$ thereby warranting its implementation in future revisions of current SE(T) test practices as the preferred compliance solution for this specimen geometry.

3.3. J-CTOD relationships

In the experimental determination of a $\delta - \Delta a$ response in which the CTOD-values are estimated directly from the measured J-values, convenient and accurate $J-$CTOD relationships are required. However, since the plastic hinge model and the double clip-gage approach are currently the prevailing procedures to determine the CTOD in several fracture test methods, only limited $J-$CTOD relationships are available. Letting $\sigma_0 = \sigma_f$ in previous Eq. (9) such that $m = J/(\delta\sigma_f)$, some relevant $J-$CTOD relationships are provided as follows.

3.3.1. SE(B) specimen

- ASTM E1820 [4]

$$m = A_0 - A_1\left(\frac{\sigma_{ys}}{\sigma_{uts}}\right) + A_2\left(\frac{\sigma_{ys}}{\sigma_{uts}}\right)^2 - A_3\left(\frac{\sigma_{ys}}{\sigma_{uts}}\right)^3, \quad 0.45 < a/W \le 0.7 \tag{35}$$

with

$$A_0 = 3.18 - 0.22(a/W) \tag{36}$$

$$A_1 = 4.32 - 2.23(a/W) \tag{37}$$

$$A_2 = 4.44 - 2.29(a/W) \tag{38}$$

$$A_3 = 2.05 - 1.06(a/W) \tag{39}$$

- Kirk and Wang (K&W) [46]

$$m = 1.221 + 0.793\left(\frac{a}{W}\right) - 1.4180\left(\frac{a}{Wn}\right) + \frac{2.751}{n}, \quad 0.05 < a/W \le 0.75 \tag{40}$$

in which n is the Ramberg-Osgood strain hardening exponent already defined previously.

Fig. 6(a) compares the variation of parameter m with a/W for a moderate hardening material with $E/\sigma_{ys} = 500$ and $n = 10$, which typifies a common API X60 pipeline steel; here, the tensile strength, σ_{uts}, entering into Eq. (35) is estimated by simply adopting the relationship $\sigma_{uts} = \sigma_{ys}[(500N)^N/\exp(N)]$ with $N = 1/n$ [1,55]. Not surprisingly, both expressions define a linear relationship between m and a/W in which m increases with increased crack size in the SE(B) specimen. For the moderate hardening material considered with $n = 10$, the ASTM E1820 [4] formulation provides slightly larger m-values.

3.3.2. Clamped SE(T) specimen

- Shen and Tyson (S&T) [30]

$$m = \begin{cases} m_c, & P \le P_Y \\ m_c - m_p[(P/P_Y) - 1], & P > P_Y \end{cases}, \quad 0.2 < a/W \le 0.5 \tag{41}$$

where $P_Y = B_N(W - a)\sigma_f$ is the specimen limit load and B_N defines

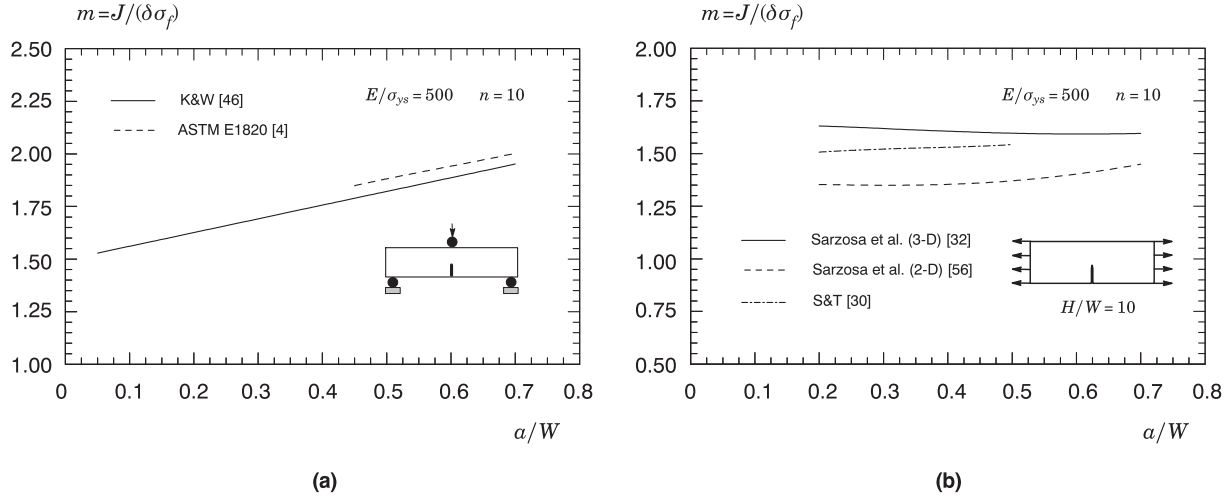

Fig. 6. Variation of parameter m with a/W for a moderate hardening material with $E/\sigma_{ys} = 500$ and $n = 10$: (a) Standard 3P SE(B) specimens. (b) clamped SE(T) specimens with $H/W = 10$.

the net specimen thickness. In the above, parameters m_c and m_p are given by

$$m_c = A_1(a/W) + A_2 \tag{42}$$

$$m_p = B_1(a/W) + B_2 \tag{43}$$

in which

$$A_1 = -0.1293 + 0.1152n - 0.00986n^2 + 0.000263n^3 \tag{44}$$

$$A_2 = 3.0867 - 0.297n + 0.0194n^2 - 0.000427n^3 \tag{45}$$

$$B_1 = 1.0169 - 0.0634n + 0.00567n^2 - 0.000200n^3 \tag{46}$$

$$B_2 = 0.6969 - 0.1216n + 0.01487n^2 - 0.000393n^3 \tag{47}$$

- Sarzosa and Ruggieri [56] (Plane-strain analysis)

$$m = 1.147 - 0.420(a/W) + 0.672(a/W)^2 + \frac{2.859}{n} - 0.002n \quad , \quad 0.2 < a/W \leq 0.7 \tag{48}$$

- Sarzosa et al. [32] (3-D analysis for side-grooved models)

$$m = 1.1171 - 0.2777(a/W) + 0.2218(a/W)^2 + 3.4824 \cdot n^{-1} - \\ -0.0012n + 1.6911sg - 1.1942sg^2 \quad , \quad 0.2 < a/W \leq 0.7 \tag{49}$$

In the above expressions, sg denotes the side-groove fraction defined by $sg = 1 - (B_N/B)$ in Sarzosa et al. [32]. It also deserves mention that the original plane-strain expression for parameter m provided in Sarzosa and Ruggieri [56] was actually derived based on σ_0 taken as the material yield stress, σ_{ys}, in previous Eq. (9). In the above Eq. (48), however, those results were manipulated into the form $m = J/(\delta\sigma_f)$, which is consistent with the framework adopted here while, at the same time, facilitating comparisons with other expressions.

Fig. 6(b) compares the variation of parameter m with a/W derived from these expressions for an $n = 10$ material representing again a typical API X60 pipeline steel in which the 3-D results of Sarzosa et al. [32] consider a side-grooved specimen with 15 % side-grooves (also note that the Sarzosa et al. [32] analyses cover 3-D models with $W = B$ and specimen thickness, B, ranging from 12.7 mm to 25.4 mm). The variation of parameter m with increased a/W-ratio corresponding to the Shen and Tyson [30] was obtained by considering a specimen geometry having $W = B = 15$ mm and 15 % side-grooves. Here, because of the dependence of parameter m on the applied load, a fixed ratio of $P/P_Y = 1.25$ was assumed to determine m in Eq. (41), which is in accord with average values for P/P_Y with $P > P_Y$ found in typical fracture resistance tests conducted by Ruggieri and co-workers (see, *e.g.*, Mathias et al. [7] and Sarzosa et al. [33]). Since the term $[(P/P_Y) - 1]$ affects only parameter m_p, which is often much smaller than parameter m_c, it does not change significantly the variation of m with a/W thereby providing comparable results with the m-values derived from the Sarzosa et al. [32] analyses. In contrast to the results shown in Fig. 6(a) for the SE(B) specimen, parameter m for the SE(T) specimens depends rather weakly on the crack size. Observe that the m results from Sarzosa et al. [32] (which correspond to 3-D analyses conducted on side-grooved models) are slightly above the m-values from the S&T [30] results thereby producing slightly more conservative crack growth resistance curves. Indeed, this is exactly the behavior found by Sarzosa et al. [32] when determining the fracture resistance response in terms of CTOD – Δa data for an X80 pipeline girth weld. Overall, these results seem to favor the adoption of either the 3-D formula of Sarzosa et al. [32] or Shen and Tyson [30] to determine conservative CTOD-resistance curves derived from J for this specimen geometry.

4. Constraint effects in SE(T) and SE(B) specimens

Much research in the last $10 \sim 20$ years has convincingly demonstrated the strong effects of specimen geometry and loading mode (bending vs. tension) on fracture behavior for ferritic structural steels in the ductile-to-brittle (DBT) transition region as well as in the upper shelf region. At increased loads in a finite body, such as a cracked specimen or structure, the initially strong small scale yielding (SSY) fields gradually change to fields under large scale yielding (LSY) as crack-tip plastic zones increasingly merge with the global bending plasticity on the nearby traction free boundaries [1,3]. This phenomenon, often termed loss of constraint, contributes to the apparent increased toughness of shallow-cracked and tension loaded geometries observed in fracture testing [5–7]. Previous studies [21,51,57,58] have characterized the changes of crack-front stress fields with increased loading for common fracture specimens using the $J - Q$ methodology to quantify effects of constraint loss on fracture behavior - readers are referred to the work of Dodds et al. [58] for a review and more complete discussion on the $J - Q$ methodology. This section repeats the major results of Ruggieri and co-workers [22,56,59] to examine the constraint variations in terms of $J - Q$ trajectories for plane-strain models of SE(B) and clamped SE(T) fracture specimens with varying crack sizes for moderate hardening material representative of a common pipeline steel. The section begins with descriptions of crack front constraint for SE(B) and clamped SE(T) specimens for stationary cracks and then explores an extension of the $J - Q$ approach to include effects of ductile tearing on crack-tip constraint which potentially impact crack growth resistance behavior for these specimen configurations.

4.1. J-Q trajectories for stationary cracks

The evolution of crack-tip stress triaxiality with J described here compare $J - Q$ trajectories derived from plane-strain analyses conducted on SE(B) and clamped SE(T) fracture specimens with varying crack sizes. The results presented in this section consider a typical API 5L Grade X70 pipeline steel with 484 MPa yield stress at room temperature (20°C) and relatively moderate-to-low hardening properties as characterized by $\sigma_{uts}/\sigma_{ys} \approx 1.22$. Hippert and Ruggieri [60] and Ruggieri [59] provide the engineering stress-strain response for this material. Results for other strain hardening properties do not provide further insight and are not shown here in interest of space (readers are referred to Sarzosa and Ruggieri [22] for full details). The finite element models constructed for the plane-strain analyses of the SE(B) and clamped SE(T) specimens employ a conventional mesh configuration having a focused ring of elements surrounding the crack front in which a small key-hole at the crack tip with radius of 0.0025 mm to enhance computation of J-values at low deformation levels. A typical half-symmetric model of the fracture specimens has one thickness layer of 1300 8-node, 3D elements (~2800 nodes) with plane-strain constraints ($w = 0$) imposed on each node. The finite element code WARP3D [61] provides the necessary numerical solutions to compute the $J - Q$ trajectories for the analyzed fracture specimens.

Fig. 7 displays the general effects of specimen geometry and

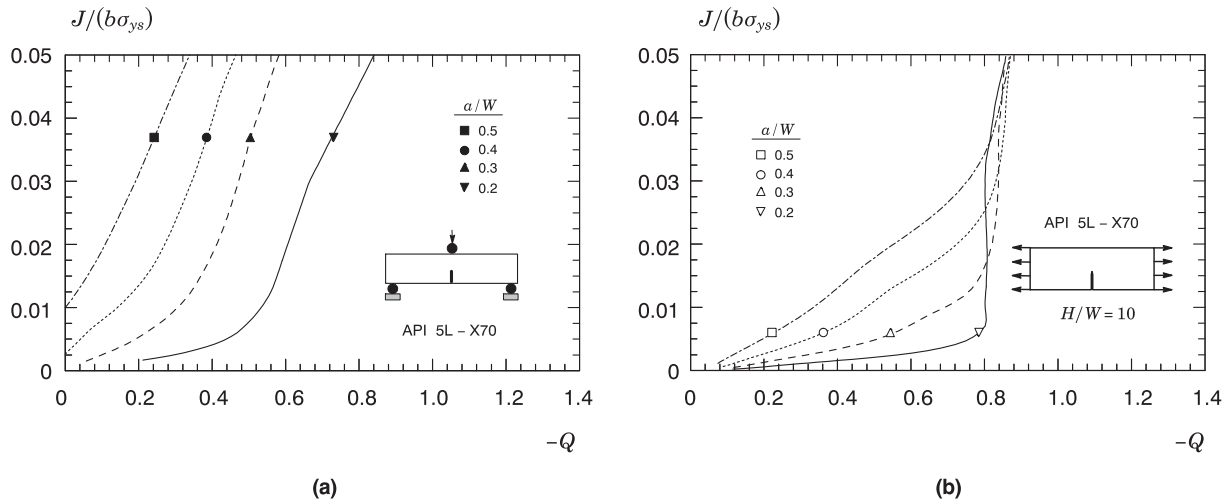

Fig. 7. Comparison of $J-Q$ trajectories with varying crack sizes for the API X70 steel: (a) 3-point SE(B) specimen. (b) Clamped SE(T) geometry with $H/W = 10$.

loading mode on the $J-Q$ trajectories for standard SE(B) specimens and clamped SE(T) configurations. In all plots, Q is defined by

$$Q = \frac{\sigma_{yy}^{FB} - \sigma_{yy}^{SSY}}{\sigma_{ys}} \tag{50}$$

in which the difference field between the fracture specimen, σ_{yy}^{FB}, and the high triaxiality reference small scale yielding (SSY) solution, σ_{yy}^{SSY}, described by $\sigma_{yy}^{FB} - \sigma_{yy}^{SSY}$ is conventionally evaluated at the normalized crack-tip distance $r = 2J/\sigma_{ys}$ whereas J is normalized by $b\sigma_{ys}$ (observe that J is plotted against $-Q$ to maintain positive scales). Consider first the evolution of Q with normalized J for the standard SE(B) specimen with varying a/W-ratio displayed in Fig. 7(a). Here, the Q-values depend markedly on crack size. For the deeply cracked SE(B) specimen with $a/W = 0.5$, the Q-parameter is positive at low load levels (note that the corresponding curve crosses the vertical axis of the plot at $J/(b\sigma_{ys}) \approx 0.01$) and gradually changes to negative values with increased levels of J. In contrast, the shallow-crack SE(B) specimen reveals large negative Q-values almost immediately upon loading. Here, values for parameter Q ranging from $-0.4 \sim -0.8$ are associated with substantial reduction in the opening near-tip stresses for this specimen early in the loading. Consider now the $J-Q$ trajectories for the clamped SE(T) specimen with $H/W = 10$ and varying a/W-ratios shown in Fig. 7(b). A different picture now emerges as the corresponding Q-values become highly negative at relatively small load levels, particularly for the shallow-cracked configurations ($a/W \approx 0.2 \sim 0.3$). An interesting development provided by these results is that all curves converge to a fixed Q-value of about 0.8. Further, observe in Fig. 7(a) that the shallow-cracked SE(B) specimen with $a/W = 0.2$ displays Q-values in the range $-0.6 \sim -0.8$ which is precisely the range of values for parameter Q in all analyzed clamped SE(T) specimens at larger load levels ($J/(b\sigma_{ys}) \approx 0.03$). Such behavior provides a particularly interesting result in that the shallow-cracked SE(B) specimen and all analyzed SE(T) configurations have similar levels of constraint at larger values of J thereby plausibly providing similar crack growth resistance curves as will be taken up next.

4.2. J-Q trajectories for growing cracks

The $J-Q$ trajectories for the SE(B) and SE(T) specimens based on a stationary crack analysis may not reflect changes in the near-tip stresses due to increased crack growth. In particular, since constraint loss with increased plastic deformation is potentially offset by the elevation in near-tip stresses due to steady growth of the crack, correlation of fracture behavior based on a stress triaxiality parameter defined for a stationary crack can be somewhat elusive. To examine ductile tearing effects on the evolution of crack-tip constraint with J for the SE(B) and clamped SE(T) specimens, the results presented here follow Ruggieri [59] and are derived from crack growth analyses conducted on plane-strain models for SE(B) and clamped SE(T) configurations incorporating the computational cell methodology proposed by Xia and Shih [62] (see also Ruggieri and Dodds [63]). These analyses consider the engineering stress-strain response for the API 5L Grade X70 pipeline steel tested by Hippert and Ruggieri [60] already briefly described in previous section. Hippert and Ruggieri [60] and Ruggieri [59] also report fracture toughness tests conducted on C(T) specimens to measure crack growth resistance curves in terms of $J-\Delta a$ for this material - these experimentally measured fracture resistance curves were employed to calibrate the key cell model parameters, including the initial volume fraction, $f_0 = 0.0005$ for the tested API X70 pipeline steel (see Sarzosa and Ruggieri [22] for full details of the crack growth analysis and cell model calibration).

Fig. 8(a) displays the computed crack growth resistance curves for the clamped SE(T) configuration with varying a/W-ratio for the calibrated cell parameter, $f_0 = 0.0005$. The resistance curves are essentially the same in the "blunting line" region ($\Delta a \lesssim 0.2$ mm) and then rise steadily with increased J-values. It can be seen that the resistance curves depend rather weakly on the a/W-ratio. In particular, note that the fracture resistance behavior for the deeply cracked SE(T) specimens with $a/W = 0.4 \sim 0.5$ are almost indistinct from each other. Fig. 8(b) provides $J-\widehat{Q}$ trajectories for the clamped SE(T) specimens with different crack sizes, which now incorporate effects of crack growth on the evolving near-tip stresses as characterized by parameter $\widehat{Q}$ defined by

$$\widehat{Q} \equiv \frac{\left(\sigma_{yy}^{FB}\right)_{\Delta a} - \left(\sigma_{yy}^{SSY}\right)_{\Delta a=0}}{\sigma_{ys}} \tag{51}$$

where the difference field described is now evaluated at the *current* normalized crack-tip distance, $\widehat{r} = 2J/\sigma_{ys}$, that represents the location of a material point ahead of the advancing crack tip. Similar to the previous analyses, J is normalized by $b\sigma_{ys}$ (observe again that J is plotted against $-\widehat{Q}$ to maintain positive scales). At

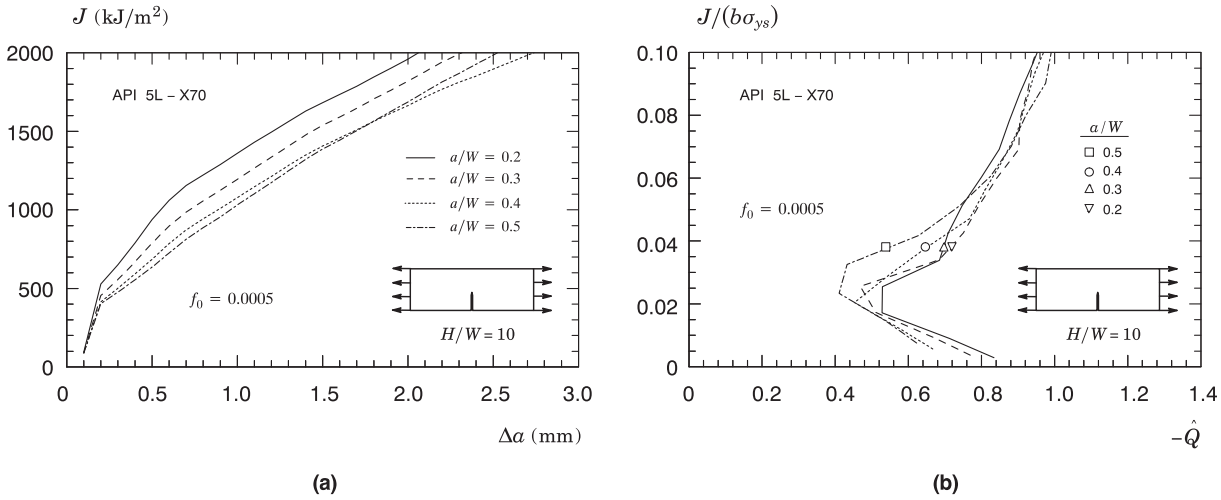

Fig. 8. Computed fracture behavior for clamped SE(T) specimens made of API X70 steel with $H/W = 10$ and varying crack sizes: (a) Crack growth resistance curves. (b) $J - \widehat{Q}$ trajectories.

early stages of loading defined by $J/(b\sigma_{ys}) \approx 0.02$, there is clearly an increase in crack-tip constraint relative to the stationary crack analysis as the $\widehat{Q}$-values vary from -0.8 to -0.4. Thereafter, all curves virtually merge into one single curve which shows that the constraint levels with increased crack growth for this specimen are almost independent of crack size (as measured by the a/W-ratio).

Attention is now directed to the effects of crack growth on fracture behavior for the SE(B) specimen. Fig. 9(a) shows the computed crack growth resistance curves for the shallow ($a/W = 0.2$) and deeply-cracked ($a/W = 0.5$) SE(B) configurations. Fig. 9(b) displays $J - \widehat{Q}$ trajectories for these SE(B) specimens including effects of crack growth. The significant features include: (1) effects of crack size (a/W-ratio) on the resistance curves are more prominent for this specimen geometry; (2) there is also no effect in the "blunting line" region of the resistance curves for both the shallow and deeply cracked configurations and (3) after an increase in crack-tip constraint at early stages of loading, the rising $J - \widehat{Q}$ trajectories for both specimen geometries differ significantly; here the $\widehat{Q}$-values for the SE(B) specimen with $a/W = 0.2$ vary from -0.3 to -0.8 over almost the entire range of loading (characterized by J) considered. This last feature provides a particularly interesting result in that the constraint levels with increased crack growth for the shallow-cracked SE(B) specimen compare well with the corresponding constraint levels for the clamped SE(T) specimens displayed in previous Fig. 8(b) thereby providing further support to the experimental results for an X80 pipeline girth weld taken up next.

While there are obvious limitations associated with the use of the Q-parameter as a highly robust descriptor of the evolution of crack-tip constraint for a growing crack, it does capture the difference field of the growing crack with reference to the high constraint SSY fields for a stationary crack. Indeed, the extended work of Sarzosa and Ruggieri [22] shows a more prominent effect of ductile tearing on the evolving levels of crack -tip constraint for deeply-cracked bend specimens than in shallow-crack bend specimens and in clamped SE(T) specimens. Moreover, their investigation also supports the arguments that shallow crack SE(B) specimens with crack sizes in the range $a/W \approx 0.2$ provide fracture response described by J-resistance curves in good agreement with the corresponding fracture behavior of circumferentially cracked pipes.

5. Fracture resistance results

The following sections provide key results of crack growth

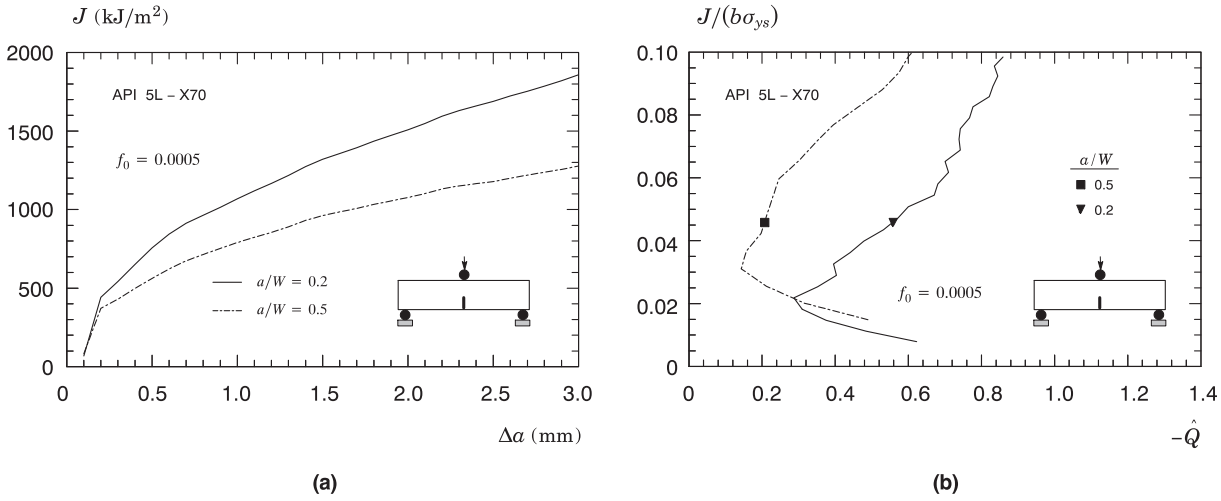

Fig. 9. Computed fracture behavior for 3P SE(B) specimens made of API X70 steel with varying crack sizes: (a) Crack growth resistance curves. (b) $J - \widehat{Q}$ trajectories.

resistance testing conducted on low constraint fracture specimens extracted from typical pipe girth welds. Primary attention is given to the effects of geometry and loading mode on J-resistance curves based on the use of clamped SE(T) and shallow-crack SE(B) geometries. The presentation considers measured experimental data from fracture testing performed on a girth weld made of a typical X80 pipeline steel and a girth weld of a X65 pipe internally clad with a nickel-chromium corrosion resistant alloy (CRA). In both cases, the evaluation procedure of fracture resistance curves briefly outlined in Section 2 is used in conjunction with the UC procedure to describe ductile response in terms of $J-\Delta a$ and CTOD $-\Delta a$ data.

5.1. X80 girth weld

Mathias et al. [7] have carried out a series of fracture experiments for a girth weld made of an API 5L X80 pipeline steel. They tested weld centerline notched specimens having two widely different geometries: (1) a clamped SE(T) specimen with fixed overall geometry and crack length to width ratio defined by $a/W=0.4$, $H/W=10$ with thickness $B=14.8$ mm and width $W=14.8$ mm; (2) a standard 3P bend specimen with $a/W=0.25$, thickness $B=14.8$ mm, width $W=14.8$ mm and span $S=4W$. These fracture specimens have a straight notch at weld centerline with the notch plane machined from the cap toward the root. After fatigue pre-cracking, both specimen geometries were side-grooved to a depth of $0.075B$ on each side to promote uniform ductile growth over the thickness. Because the level of crack-tip constraint in clamped SE(T) specimens is weakly dependent on crack size (see previous results in Section 4), the tested SE(T) geometry with $a/W=0.4$ is very representative of the crack resistance behavior for this crack configuration having other a/W-ratios.

The tested weld joint was made from the API X80 pipe using the FCAW process in the 1G (flat) position with a single V-groove configuration. Mechanical tensile tests conducted on the weld metal (WM) and base plate material (BM) at room temperature (20°C) provided the following average tensile properties for: $\sigma_{ys}^{BM}=609$ MPa and $\sigma_{uts}^{BM}=679$ MPa; $\sigma_{ys}^{WM}=716$ MPa and $\sigma_{uts}^{WM}=750$ MPa. The measured tensile properties indicate that the weldment overmatches the base plate material by only 18% at room temperature and, thus, the mechanical properties considered in the present study are those for the base plate material. Based on Annex F of API 579 [55], the Ramberg-Osgood strain hardening exponents describing the stress-strain response for the base plate material is estimated as $n_{BM}=20.3$.

Fig. 10 show the measured resistance curves for the tested crack configurations with different specimen geometries and a/W-ratios. These fracture data were obtained using the expressions for factor η and compliance solutions defined by Eqs. (13), (17) and (28) for the SE(B) specimen and Eqs. (25), (26) and (32) for the clamped SE(T) geometry. The scatter in the measured resistance curves is slightly larger than one would expect for a conventional ductile tearing test, particularly in the case of the shallow crack bend geometry, possibly due to the rather strong heterogeneity of the weld metal. Nevertheless, the experimental results are rather conclusive in that the fracture resistance values for the shallow-crack SE(B) configuration are generally similar to the corresponding values for the clamped SE(T) specimens. Moreover, it is also evident that the J-resistance data for the shallow crack bend specimen compare relatively well with those corresponding to the clamped SE(T) configuration. Here, a rough estimate of the fracture toughness value at $\Delta a=1$ mm for the shallow-crack SE(B) specimen yields $J\approx 600$ kJ/m^2 whereas for the clamped SE(T) specimen one would obtain $J\approx 550$ kJ/m^2. Mathias et al. [7] also provide fracture resistance data for the shallow-crack SE(B) specimen for which the J-values were obtained on the basis of η-factors derived from 3-D

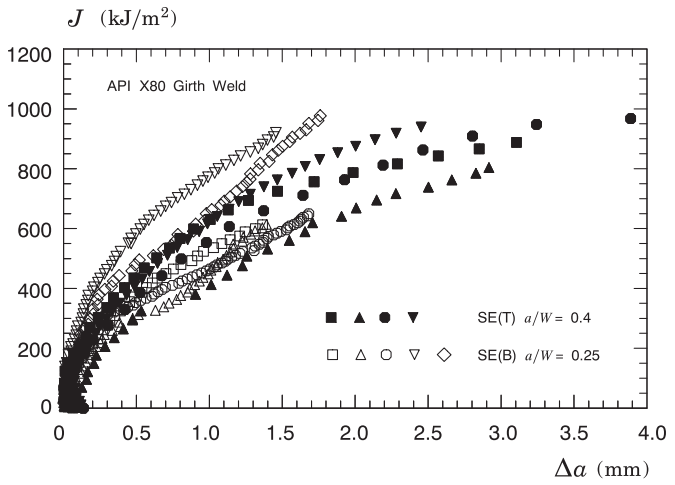

Fig. 10. Comparison of J-resistance curves for the tested shallow-crack SE(B) specimens and clamped SE(T) geometries.

analysis conducted on 3P SE(B) geometries with $B=W=14.8$ mm. For this case, the experimental fracture resistance curves fall slightly below (differences of $\approx 10\sim 15\,\%$) the corresponding $J-\Delta a$ data shown in the plots of Fig. 10 - however, the overall trends remain essentially the same.

Evaluation of ductile fracture response for the tested pipeline girth weld in terms of CTOD $-R$ curves derived from the SE(T) testing is also of interest. Fig. 11 shows the measured CTOD resistance curves for selected SE(T) specimens already displayed in previous Fig. 10. Here, the CTOD resistance data is determined as follows: 1) First, the J-values are evaluated using the procedure outlined above in which the plastic η-factors based on CMOD and LLD, η_{J-CMOD} and η_{J-LLD}, and the crack length estimation equations are derived from Mathias et al. [7]; 2) Next, the corresponding CTOD-values are determined using the $J-$CTOD relation defined by Eq. (49) from Sarzosa et al. [32] in which the *current* crack length (rather than the original crack size) is used. To provide additional support and further verification of the J-CTOD relations presented in the present work, Fig. 11 also includes the CTOD $-R$ curve obtained from a related $J-$CTOD formulation developed by S&T [30] and defined by Eq. (41) - here, it is understood that, while the S&T expression is strictly valid in the range $0.2\le a/W\le 0.5$, Eq. (41)

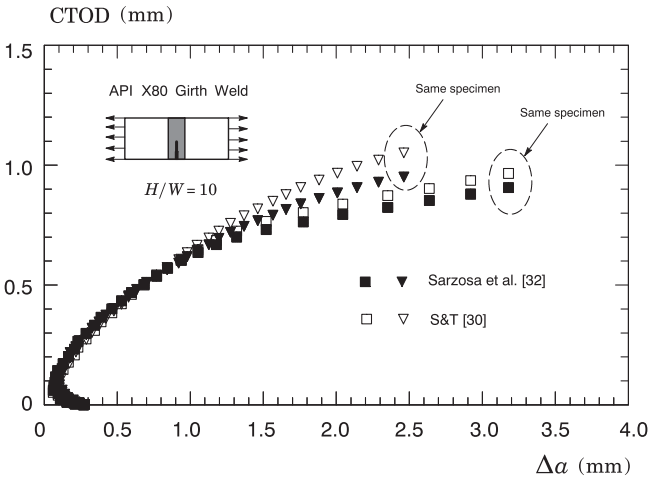

Fig. 11. Comparison of J-resistance curves for the tested shallow-crack SE(B) specimens and clamped SE(T) geometries.

can reasonably be used for higher a/W-ratios (corresponding to $a/W = 0.57$ and 0.62 for both specimens displayed in the figure) as implied by a simple extrapolation of the results shown in previous Fig. 6. These analyses show that the CTOD resistance curves using the $J-$CTOD relationships developed by Sarzosa et al. [32] lie only slightly below the corresponding curves derived from using the m-values from S&T [30].

5.2. Dissimilar nickel-chromium girth welds for clad line pipes

Sarzosa et al. [33] performed unloading compliance tests at room temperature on weld centerline notched SE(T) specimens extracted from a girth weld of a typical API 5L X60 pipe internally clad with a nickel-chromium corrosion resistant alloy (CRA). Again, these fracture specimens have a straight notch at weld centerline with the notch plane machined from the cap toward the root. The tested weld joint was made from an 8-inch pipe (203 mm outer diameter) having overall thickness, $t_w = 19$ mm, which includes a clad layer thickness, $t_c = 3$ mm. The material of the external pipe has a high yield stress of 620 MPa and low hardening properties with $\sigma_{uts}/\sigma_{ys} \approx 1.13$, whereas the inner clad layer has yield stress of 462 MPa and relatively high hardening behavior with $\sigma_{uts}/\sigma_{ys} \approx 1.36$ - the measured tensile properties indicate that the weldment undermatches the base plate material by ≈ 25 % at room temperature.

The tested SE(T) specimens have $a/W = 0.3$ and $H/W = 10$ with thickness $B = 16$ mm, width $W = 16$ mm and clamp distance $H = 160$ mm. After fatigue pre-cracking, the specimens were side-grooved to a net thickness of $\sim 85\%$ the overall thickness (7.5% side-groove on each side) to promote uniform crack growth. The test program covered four specimens, one of them instrumented with a double clip-gage fixture as required for CMOD measurements at two different points (refer to Fig. 1(a)) for evaluation of the CTOD using the DCG method as previously described in Section 2.3. It is of interest to note that the double clip-gage fixture in this specimen is used only to determine the CTOD not J, which is evaluated on the basis of the same procedure utilized to determine the other J-resistance curves.

Because of the dissimilar nature of the two materials, including the clad layer thickness, from which the weld centerline notched SE(T) specimens are made, Sarzosa et al. [33] also derived an improved $J-$CTOD relationship. By performing full 3-D analysis of the tested fracture specimens incorporating the mismatch behavior in flow properties between the weld metal, including the clad layer, and the base plate material, they arrived at the dependence of parameter m entering into Eq. (9) given by

$$m = 1.932 - 1.845(a/W) + 1.654(a/W)^2, \quad 0.1 \le a/W \le 0.7 \tag{52}$$

which is used next to obtain the measured CTOD resistance curves.

Figs. 12 and 13 display the 4 resistance curves for the dissimilar nickel-chromium girth weld measured by Sarzosa et al. [33] in terms of $J-\Delta a$ and CTOD $-\Delta a$ data. Consider first J-resistance curves shown in Fig. 12 in which J and Δa are evaluated using plane-strain solutions for η and μ (as described by Eqs. (25), (26) and (32 from Mathias et al. [7]) applicable to a homogeneous material having flow properties corresponding to those for the weld metal. This is equivalent to assuming that the entire bulk of the specimen has the same flow properties as the weld metal - a condition usually referred to as all weld metal (AWM). As the figure indicates, the J-resistance curve represented by the solid symbol corresponds to one of the specimens which was instrumented with a double clip-gage fixture for subsequent evaluation of CTOD. Apart from the

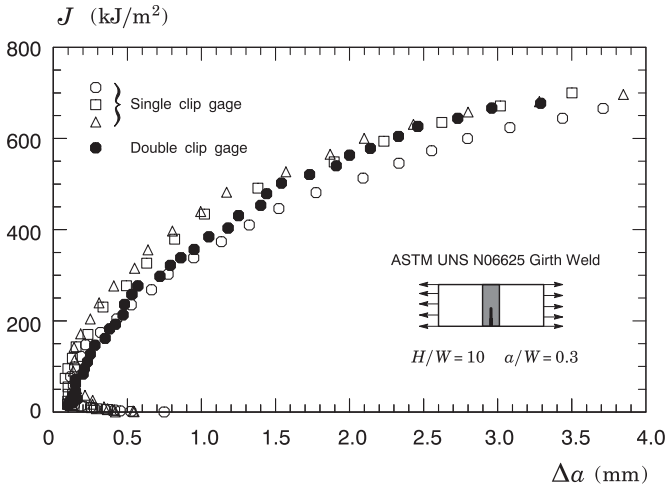

Fig. 12. J-resistance curves for the tested clamped SE(T) specimens based on plane-strain η-factors for a homogeneous material (AWM). The solid symbol corresponds to one of the specimens which was instrumented with a double clip-gage fixture (used only to determine the CTOD not J).

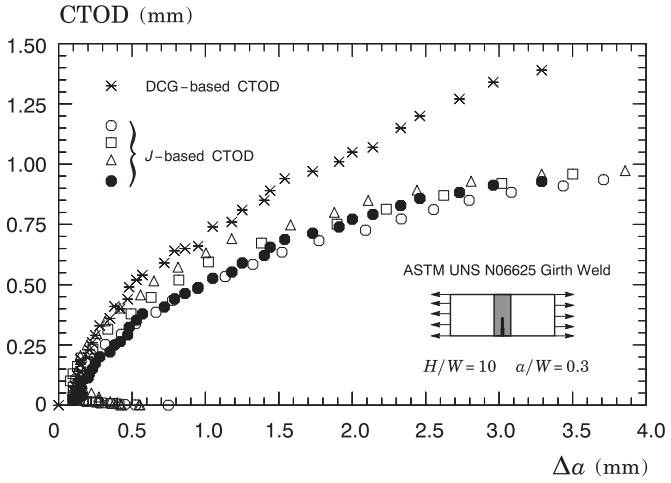

Fig. 13. CTOD-resistance curves for the tested clamped SE(T) specimens derived from the $J-$CTOD relationship defined by Eq. (9) in which parameter m is evaluated by means of Eq. (52). The plot also includes a CTOD-resistance curve derived from the double clip-gage (DCG) method for the tested SE(T) specimen instrumented with a double clip-gage fixture.

"crack backup" (or apparent negative crack growth) observed in the initial part of the $J-R$ curves for all tested specimens, the overall trend of increased J-values with increased amounts of ductile tearing is evident in this plot - observe, however, that the resistance curves do show some signs of leveling off at large amounts of ductile tearing.

Consider next the CTOD $-R$ curves shown in Fig. 13 in which the crack tip opening displacement is determined from the $J-$CTOD relationship defined by Eq. (52). Moreover, the fracture resistance in terms of CTOD based on the DCG method is also included in the plot. Here, only the load-displacement data measured from testing the specimen equipped with a double clip-gage fixture is used to generate that CTOD $-R$ curve displayed in Fig. 13. The DCG-based resistance curve is consistently higher than the CTOD $-R$ curves based on J, particularly for larger amounts of stable crack growth, say $\Delta a \gtrsim 1.5$ mm - this behavior is entirely consistent with recent experimental observations by Zhu et al. [36] for an A36 steel. It can be seen that differences between both methods range from $\sim 25\%$

for $\Delta a = 1.5$ mm to $\sim 45\%$ for $\Delta a = 3$ mm. Observe, however, that the CTOD resistance data based on DCG measurements increase steadily with crack growth for $\Delta a > 1.0$ mm such that the corresponding tearing modulus, which can be simply defined as $d\delta/da$ [1], remains essentially constant. In contrast, the J-based CTOD resistance curves also increase with increased Δa but at a much lower rate as characterized by much smaller values of $d\delta/da$, particularly at larger amounts of ductile tearing. Allowing for some uncertainties and difficulties associated with double clip-gage measurements, these results seem generally consistent with previous observations [33] that, because the developed $J-$CTOD relationship does include effects of crack growth on J, the associated CTOD resistance curve should be lower than the DCG-based resistance curve. Moreover, Sarzosa et al. [33] argue that, at large deformation levels (which correspond to larger amounts of stable crack growth), much of the total work done by the applied (remote) loading is likely dissipated into background plasticity thereby reducing the plastic contribution to the strain energy for the cracked body in terms of J. In contrast, because the CTOD based on DCG derives from a rather simple measurement of the relative displacements of the crack profile (refer again to Fig. 1(b)), it keeps increasing with increased loading. Also observe that, as already briefly discussed in Section 2.3, the DCG mounting fixture is typically installed at a distance x_0 from the notch flank, as shown in previous 1(b), which can result in an *apparent* offset of the crack flank thereby potentially increasing the measured CTOD, even soon after the onset of crack initiation as 13 reveals. Thus, it becomes clear that the DCG-based resistance curve results in non-conservative toughness values at fixed amounts of stable crack growth thereby potentially impacting adversely ECA assessments.

6. Concluding remarks

This article provides a brief review of current progress in fracture resistance test procedures to measure crack growth properties using low constraint fracture specimens represented by shallow-crack SE(B) specimens loaded under three-point bending and single edge notch tension SE(T) specimen with fixed-grip loading (clamped ends). Much recent research and on-going work have shown that these test methods are now becoming a mature procedure for accurate measurements of fracture resistance properties in ductile materials, including primarily crack growth resistance curves for pipeline girth welds. In particular, the experiments and fracture resistance data described in this paper show the effectiveness of the UC procedure to characterize ductile tearing properties of pipeline girth weld materials which serve as a basis for ductile tearing assessments in ECA procedures applicable to a large class of structural components. Further, the analyses and test results described here also provide support to the use of shallow-crack bend specimens as an alternative fracture specimen to measure crack growth properties for pipeline girth welds and similar mechanical configurations. While there remain a number of unresolved questions, such as the proper and best choices of plastic η-factors and compliance equations, substantial progress has been recently made in development of fracture testing standards to describe procedures for the mechanical testing and data analysis.

Undoubtedly, one of the most controversial issue related to fracture resistance measurements in pipeline girth welds is whether a CTOD $-R$ curve should be derived from first evaluating the J-integral and then converting it to the corresponding CTOD-value or from using the double clip-gage (DCG) technique. The limited results shown here suggest that, even though both $J-R$ and CTOD $-R$ curves suffice to characterize well the crack growth resistance behavior for the tested materials provided accurate and robust $J-$CTOD relationships are available, evaluation of CTOD based on the double clip-gage technique does provide higher resistance curves and, thus, non-conservative toughness values at fixed amounts of stable crack growth. Nevertheless, it is well to keep in mind that this drawback could be circumvented to a large extent by adopting a geometrically consistent definition of crack tip loading in terms of CTOD that would closely relate to the CTOD measurement derived from the DCG method. Thus, for example, in a defect assessment procedure for a pipeline girth weld in which the ductile tearing properties for the weld metal are described by a CTOD $-R$ curve obtained from the DCG method, the corresponding crack driving force would preferably be defined in terms of the CTOD numerically determined from measurements of crack opening displacements (COD) at two different points on the crack flank of a finite element model for the pipeline girth weld, thereby yielding a geometrical relationship between the CTOD and both measured COD-values similar to that used in the DCG procedure. Clearly, this issue remains open and appears central to develop a more robust and efficient fracture resistance evaluation procedures. Overall, this study shows that shallow-crack SE(B) specimens and clamped SE(T) geometries are highly effective in producing geometry-dependent fracture resistance data derived from the UC procedure, which are representative of low constraint structural components containing crack-like flaws, including pipeline girth welds.

Acknowledgments

This investigation is primarily supported by the Brazilian Council for Scientific and Technological Development (CNPq) through Grant 306193/2013-2. The author also acknowledges the Brazilian State Oil Company (Petrobras) for providing additional support for the work described here and for making available the experimental data. Helpful discussions with Dr. E. Hippert (Petrobras) are also acknowledged.

References

[1] Anderson TL. Fracture mechanics: fundaments and applications. third ed. Boca Raton, FL: CRC Press; 2005.
[2] Joyce JA. Manual on elastic-plastic fracture: laboratory test procedure. ASTM Manual Series MNL 27. ASTM International; 1996.
[3] Hutchinson JW. Fundamentals of the phenomenological theory of nonlinear fracture mechanics. J Appl Mech 1983;50:1042–51.
[4] American Society for Testing and Materials. Standard test method for measurement of fracture toughness. ASTM E1820–15. 2015.
[5] Joyce JA, Hackett EM, Roe C. Effects of crack depth and mode loading on the J-R curve behavior of a high strength steel. In: Underwood JH, Schwalbe K-H, Dodds RH, editors. Constraint effects in fracture. Philadelphia: American Society for Testing and Materials; 1993. p. 239–63. ASTM STP 1171.
[6] Joyce JA, Link RE. Effects of constraint on upper shelf fracture toughness. In: Reuter WG, Underwood JH, Newman J, editors. Fracture mechanics. Philadelphia: American Society for Testing and Materials; 1995. p. 142–77. ASTM STP 1256.
[7] Mathias LLS, Sarzosa DFB, Ruggieri C. Effects of specimen geometry and loading mode on crack growth resistance curves of a high-strength pipeline girth weld. Int J Press Vessels Pip 2013;111–112:106–19.
[8] Pussegoda N, Tiku S, Tyson W. Measurements of crack-tip opening displacement (CTOD) and J-fracture resistance curves using single-edge notched tension (SENT) specimens. Tech. Rep. 30166-001-R01. BMT Fleet Technology; 2014.
[9] British Institution. Method of test for determination of fracture toughness in metallic materials using single edge notched tension (SENT) specimens. BS 8571. 2014.
[10] Det Norske Veritas. Fracture control for pipeline installation methods introducing cyclic plastic strain. DNV-RP-F108. 2006.
[11] Ruggieri C, Hippert E. Test procedure for fracture resistance characterization of pipeline steels and pipeline girth welds using single-edge notched tension (SENT) specimens. Tech. rep. University of São Paulo; 2015.
[12] ExxonMobil Upstream. Measurements of crack-tip opening displacement (CTOD) fracture resistance curves using single-edge notched tension (SENT) specimens. Tech. rep.. 2010.
[13] Shen G, Tyson WR. Crack size evaluation using unloading compliance in single-specimen single-edge notched tension fracture toughness testing.

J Test Eval 2009;37(4):347–57.
[14] G. Shen, J. A. Gianetto, W. R. Tyson, Measurements of J–R curves using single specimen technique on clamped SE(T) specimens, in: 19th International Offshore and Polar Engineering Conference (ISOPE), Osaka, Japan, 2009.
[15] International Organization for Standardization. Metallic materials - method of test for the determination of quasistatic fracture toughness of welds. ISO 15653–2010. 2010.
[16] Begley JA, Landes JD. The J-integral as a fracture criterion. In: Corten HT, Gallagher JP, editors. Fracture toughness. Philadelphia: American Society for Testing and Materials; 1972. p. 1–20. ASTM STP 514.
[17] Rice JR, Paris PC, Merkle JG. Some further results of J-integral analysis and estimates. In: Kaufman J, Swedlow J, Corten H, Srawley J, Heyer R, Wessel E, Irwin G, editors. Progress in flaw growth and fracture toughness testing. Philadelphia: American Society for Testing and Materials; 1973. p. 231–45. ASTM STP 536.
[18] Clarke GA, Andrews WR, Paris PC, Schmidt DW. Single specimen tests for J_{Ic} determination. In: Rice JR, Paris PC, editors. Mechanics of crack growth. Philadelphia: American Society for Testing and Materials; 1976. p. 27–42. ASTM STP 590.
[19] Zhu XK, Joyce JA. Review of fracture toughness (G, K, J, CTOD, CTOA) testing and standardization. Eng Fract Mech 2012;86:1–46.
[20] Eiber RJ, Kiefner JF. Failure of pipelines. In: Becker WT, Shipley RJ, editors. ASM handbook, vol. 11. Materials Park, OH: ASM International; 2002. p. 2791–818.
[21] Cravero S, Ruggieri C. Correlation of fracture behavior in high pressure pipelines with axial flaws using constraint designed test specimens - Part I: plane-strain analyses. Eng Fract Mech 2005;72:1344–60.
[22] Sarzosa DFB, Ruggieri C. A numerical investigation of constraint effects in circumferentially cracked pipes and fracture specimens including ductile tearing. Int J Press Vessels Pip 2014;120–121:1–18.
[23] Chiesa M, Nyhus B, Skallerud B, Thaulow C. Efficient fracture assessment of pipelines: a constraint-corrected SENT specimen approach. Eng Fract Mech 2001;68:527–47.
[24] Kanninen MF, Popelar CH. Advanced fracture mechanics. New York: Oxford University Press; 1985.
[25] Ruggieri C. Further results in J and CTOD estimation procedures for SE(T) fracture specimens - Part I: homogeneous materials. Eng Fract Mech 2012;79:245–65.
[26] Paredes M, Ruggieri C. Further results in J and CTOD estimation procedures for SE(T) fracture specimens - Part II: weld centerline cracks. Eng Fract Mech 2012;89:24–39.
[27] Cravero S, Ruggieri C. Estimation procedure of J-resistance curves for SE(T) fracture specimens using unloading compliance. Eng Fract Mech 2007;74:2735–57.
[28] Cravero S, Ruggieri C. Further developments in J evaluation procedure for growing cracks based on LLD and CMOD data. Int J Fract 2007;148:387–400.
[29] Shen G, Bouchard R, Gianetto JA, Tyson WR. Fracture toughness evaluation of high-strength steel pipe. In: ASME PVP 2008 pressure vessel and piping division conference. Chicago, IL: American Society of Mechanical Engineers; 2008.
[30] G. Shen, W. R. Tyson, Evaluation of CTOD from J-integral for SE(T) specimens, in: Pipeline Technology Conference (PTC 2009), Ostend, Belgium, 2009.
[31] M. Verstraete, S. Hertelé, K. Van Minnebruggen, R. Denys, W. De Waele, Determination of pipe girth weld fracture toughness using SENT, in: 6th International Pipeline Technology Conference, Ostend, Belgium, 2013.
[32] Sarzosa DFB, Souza RF, Ruggieri C. J-CTOD relations in clamped SE(T) fracture specimens including 3-D stationary and growth analysis. Eng Fract Mech 2015;147:331–54.
[33] Sarzosa DFB, Barbosa VS, Santos CP, Hippert E, Ruggieri C. Fracture resistance testing of dissimilar nickel-chromium girth welds for clad line pipes. Int J Fract 2017;205(2):168–88.
[34] D. Y. Park, J. P. Gravel, C. H. M. Simha, J. Liang, D. M. Duan, Fracture toughness of X70 pipe girth welds using clamped SE(T) and SE(B) single-specimens, in: 10th International Pipeline Conference (IPC 2014), Calgary, Canada, 2014.
[35] Verstraete M, De Waele W, Van Minnebruggen K, Hertelé S. Single-specimen evaluation of tearing resistance in SENT testing. Eng Fract Mech 2015;148:324–36.
[36] Zhu XK, Zelenak P, McGaughy T. Comparative study of CTOD-resistance curve test methods for SENT specimens. Eng Fract Mech 2017;172:17–38.
[37] S. Tiku, N. Pussegoda, M. GhovPuss, W. R. Tyson, A. Dinovitzer, Standardization of SENT (or SE(T)) fracture toughness measurements: Results of a round robin on a draft test procedure, in: 11th International Pipeline Conference (IPC 2016), Calgary, Canada, 2016.
[38] X. K. Zhu, T. McGaughy, A review of fracture toughness testing and evaluation using sent specimens, in: 10th International Pipeline Conference (IPC), Calgary, Canada, 2014.
[39] Zhu XK. Review of fracture toughness test methods for ductile materials in low-constraint conditions. Inter J Press Vessel Pip 2016;139–140:173–83.
[40] E. Drexler, Y.-Y. Wang, J. W. Sowards, M. D. Dvorak, SE(T) testing of pipeline welds, in: 8th International Pipeline Conference (IPC), Calgary, Canada, 2010.
[41] D. Y. Park, W. R. Tyson, J. A. Gianetto, G. Shen, R. S. Eagleson, Evaluation of fracture toughness of X100 pipe steel using SE(B) and clamped SE(T) single specimens, in: 8th International Pipeline Conference (IPC), Calgary, Canada, 2010.
[42] Tada H, Paris PC, Irwin GR. The stress analysis of cracks handbook. third ed. American Society of Mechanical Engineers; 2000.
[43] Ernst HA, Paris PC, Landes JD. Estimations on J-integral and tearing modulus T from a single specimen record. In: Roberts R, editor. Fracture mechanics: thirteenth conference. Philadelphia: American Society for Testing and Materials; 1981. p. 476–502. ASTM STP 743.
[44] Zhu XK, Leis BN, Joyce JA. Experimental estimation of J-R curves from load-CMOD record for SE(B) specimens. J ASTM Int 2008;5(5):1–15.
[45] Kirk MT, Dodds RH. J and CTOD estimation equations for shallow cracks in single edge notch bend specimens. J Test Eval 1993;21:228–38.
[46] Kirk MT, Wang Y-Y. Wide range CTOD estimation formulae for SE(B) specimens. In: Reuter WG, Underwood JH, Newman J, editors. Fracture mechanics. Philadelphia: American Society for Testing and Materials; 1995. p. 126–41. ASTM STP 1256.
[47] Kim YJ, Schwalbe K-H. On experimental J estimation equations based on CMOD for SE(B) specimens. J Test Eval 2001;29:67–71.
[48] G. H. B. Donato, C. Ruggieri, Estimation procedure for J and CTOD fracture parameters using three-point bend specimens, in: 6th International Pipeline Conference (IPC 2006), Calgary, Canada, 2006.
[49] Souza RF, Ruggieri C. Revised η-factors and J-CTOD relationships for SE(B) fracture specimens including 3-D effects and implications for fracture toughness measurements. Mater Perform Charact 2015;2(2):34–54. ASTM International.
[50] American Society for Testing and Materials. Standard test method for determination of reference temperature, T0, for ferritic steels in the transition range. ASTM E1921–16. 2016.
[51] Nevalainen M, Dodds RH. Numerical investigation of 3-D constraint effects on brittle fracture in SE(B) and C(T) specimens. Int J Fract 1995;74:131–61.
[52] Wang E, de Waele W, Hertelé S. A complementary η_{pl} approach in J and CTOD estimations for clamped SENT specimens. Eng Fract Mech 2015;147:36–54.
[53] Souza RF, Ruggieri C. Revised wide range compliance solutions for selected standard and non-standard fracture test specimens based on crack mouth opening displacement. Eng Fract Mech 2017;178:77–92.
[54] Cravero S. Evaluation of J–R-resistance curves for SE(T) fracture specimens using the unloading compliance method. Ph. D. Thesis. University of São Paulo, School of Engineering; 2007.
[55] American Petroleum Institute. Fitness-for-service. API RP-579–1/ASME FFS-1. 2007.
[56] D. F. B. Sarzosa, C. Ruggieri, Relationship between J and CTOD in SE(T) and SE(B) specimens for stationary and growing cracks, in: 10th International Pipeline Conference (IPC 2014), Calgary, Canada, 2014.
[57] Silva LAL, Cravero S, Ruggieri C. Correlation of fracture behavior in high pressure pipelines with axial flaws using constraint designed test specimens - Part II: 3-D effects on constraint. Eng Fract Mech 2006;76:2123–38.
[58] Dodds RH, Shih C, Anderson T. Continuum and micro-mechanics treatment of constraint in fracture. Int J Fract 1993;64:101–33.
[59] C. Ruggieri, Constraint effects on ductile crack growth in SE(T) and SE(B) specimens with implications for assessments of tearing resistance, in: 9th International Pipeline Conference (IPC 2012), Calgary, Canada, 2012.
[60] E. Hippert, C. Ruggieri, Experimental and numerical investigation of ductile crack extension in a high strength pipeline steel, in: ASME 2001 Pressure Vessels & Piping Conference (PVP 2001), Atlanta, GA, 2001.
[61] Healy B, Gullerud A, Koppenhoefer K, Roy A, RoyChowdhury S, Petti J, Walters M, Bichon B, Cochran K, Carlyle A, Sobotka J, Messner M, Dodds RH. WARP3D: 3-D nonlinear finite element analysis of solids for fracture and fatigue processes. Tech. rep. Urbana-Champaign: University of Illinois; 2014. http://code.google.com/p/warp3d.
[62] Xia L, Shih CF. Ductile crack growth - I: a numerical study using computational cells with microstructurally-based length scales. J Mech Phys Solids 1995;43:223–59.
[63] Ruggieri C, Dodds RH. Numerical modeling of ductile crack growth using computational cell elements. Int J Fract 1996;82:67–95.